JOURNAL OF GEOPHYSICAL RESEARCH, VOL. 112, F03S09, doi:10.1029/2006JF000567, 2007

Predictions of steady state and transient landscape morphology using sediment-flux-dependent river incision models

N. M. Gasparini,[1,2] K. X. Whipple,[2,3] and R. L. Bras[4]

Received 19 May 2006; revised 28 September 2006; accepted 21 December 2006; published 19 May 2007.

[1] Recent experimental and theoretical studies support the notion that bed load in mountain rivers can both enhance incision rates through wear and inhibit incision rates by covering the bed. These effects may play an important role in landscape evolution and, in particular, the response of river channels to tectonic or climatic perturbation. We use the channel-hillslope integrated landscape development (CHILD) numerical model with two different bedrock incision models that include the dual role of the sediment flux to explore the transient behavior of fluvial landscapes. Both models predict that steady state channel slopes increase in landscapes with higher rock uplift rates. However, the incision models predict different transient responses to an increase in uplift rate, and the behavior of each incision model depends on both the magnitude of change in uplift rate and the local drainage area. In some cases, the transient channel behavior is indistinguishable from that predicted for transport-limited alluvial rivers. In other cases, knickpoints form in some or all of the drainage network, as predicted by the detachment-limited stream power model. In all cases the response in the lower parts of the network is highly dependent on the response in the upper parts of the network as well as the hillslopes. As the upper parts of the network send more sediment downstream, channel incision rates may rise or fall, and slopes in the lower parts of the channel may, in fact, decrease at times during the transient adjustment to an increase in rock uplift rate. In some cases, channel incision in the upper parts of the network ceases during the transient while the hillslopes adjust to the new uplift rate; drainage density may also change as a function of uplift rate. Our results suggest that if the sediment flux strongly controls bedrock incision rates, then (1) the transient fluvial response will take longer than predicted by the detachment-limited stream power model, (2) changes in channel slope may be much more complex than predicted by the detachment-limited stream power model, and (3) changes in the fluvial system will be closely tied to sediment delivery from the hillslopes. Importantly, our results outline quantitative differences in system behavior produced by competing models and provide a framework for identifying locations in natural systems where differences in channel morphology can be used to discern between competing fluvial erosion models.

Citation: Gasparini, N. M., K. X. Whipple, and R. L. Bras (2007), Predictions of steady state and transient landscape morphology using sediment-flux-dependent river incision models, *J. Geophys. Res.*, *112*, F03S09, doi:10.1029/2006JF000567.

1. Motivation and Scope

[2] Understanding the behavior of bedrock channels is critical to understanding the evolution of mountainous topography and the interaction between climate and tectonics [e.g., *Howard et al.*, 1994; *Hilley et al.*, 2004; *Whipple and Meade*, 2004; *Roe et al.*, 2006]. However, in comparison with alluvial channels, relatively little is known about the controls on bedrock incision. Recently, more and more studies have focused on the processes that control fluvial incision into bedrock. These processes include chemical weathering, cavitation, plucking of bedrock blocks, and wear by suspended and bed load sediment [e.g., *Wohl*, 1993; *Hancock et al.*, 1998; *Sklar and Dietrich*, 1998; *Wohl*, 1998; *Whipple et al.*, 2000b; *Hartshorn et al.*, 2002; *Whipple*, 2004]. Similarly to alluvial channels, precipitation patterns and runoff mechanisms seem to be an important driver of the processes controlling bedrock inci-

[1]Department of Geology and Geophysics, Yale University, New Haven, Connecticut, USA.
[2]Now at School of Earth and Space Exploration, Arizona State University, Tempe, Arizona, USA.
[3]Department of Earth, Atmospheric, and Planetary Sciences, Massachusetts Institute of Technology, Cambridge, Massachusetts, USA.
[4]Department of Civil and Environmental Engineering, Massachusetts Institute of Technology, Cambridge, Massachusetts, USA.

0148-0227/07/2006JF000567$09.00

sion, especially if there are significant thresholds above which incision and sediment transport occur [e.g., *Molnar*, 2001; *Snyder et al.*, 2003a; *Tucker*, 2004]. In this study, we focus solely on how the sediment flux influences bedrock incision and channel profile evolution.

[3] The dual role that the sediment flux has in both enhancing and inhibiting bedrock incision was first discussed by *Gilbert* [1877], but very few incision models have included the sediment flux as a variable until recently [e.g., *Sklar and Dietrich*, 1998, 2004]. Instead, bedrock incision is commonly modeled as a function of shear stress or unit stream power [e.g., *Howard and Kerby*, 1983; *Howard*, 1994; *Rosenbloom and Anderson*, 1994; *Whipple and Tucker*, 1999]. With some assumptions, both the shear stress and stream power models can be expressed as a function of only two variables: drainage area and slope [e.g., *Tucker and Slingerland*, 1997; *Whipple and Tucker*, 1999]. Although the effects of sediment flux are also a function of drainage area and slope, the influence of sediment flux on incision rate is not specifically included in either the shear stress or stream power formulations. The influence of sediment flux on fluvial incision may affect the scaling relationship between incision rate and both drainage area and slope [*Sklar and Dietrich*, 1998; *Tomkin et al.*, 2003; *van der Beek and Bishop*, 2003; *Sklar and Dietrich*, 2004; *Brandon and Gasparini*, 2005].

[4] *Beaumont et al.* [1992] and *Kooi and Beaumont* [1994] proposed a bedrock incision model that includes a sediment flux term. Their under-capacity model is based on the idea that the channel has some amount of energy to expend on both transport and incision. In their model, all else being equal, a larger sediment flux means a smaller incision rate. In physical terms, their model includes the role that the sediment flux may play in hindering erosion, but not the role that the sediment flux may have in enhancing erosion rates.

[5] *Hancock and Anderson* [2002] considered a model in which sediment flux hinders erosion when sediment flux exceeds the sediment transport capacity, but their model lacked any explicit representation of the positive role of sediment flux in bedrock incision. Their model is thus similar to the hybrid models used by *Howard* [1994] and *Whipple and Tucker* [2002].

[6] *Whipple and Tucker* [2002] describe a model (based on the observations of *Sklar and Dietrich* [1998]) in which increasing sediment flux (relative to the sediment transport capacity) increases incision rates as more sediment is available to act as tools on the bed. However, at some point, increases in sediment flux shield the bed from particle impacts and incision rates begin to decline with increases in sediment flux. *Whipple and Tucker* [2002] pointed out that the details of the incision equation, specifically whether or not the incision equation includes a sediment flux term, appear not to be important in steady state conditions with a uniform rock uplift rate. Their study explored the nonsteady state behavior of channel evolution using both the detachment-limited stream power and transport-limited models, along with a hybrid mix between the two. *Whipple and Tucker* [2002] did not explore the nonsteady state behavior of channels using the sediment flux model that they presented.

[7] The nonsteady state behavior predicted using the *Whipple and Tucker* [2002] sediment flux model was later explored by *Gasparini et al.* [2006]. This study found that the sediment flux dependence can lead to a much longer response time in channels and a much more complex response in channel slopes, in comparison to the transient response described by *Whipple and Tucker* [2002] using the detachment-limited stream power model. *Gasparini et al.* [2006] show that the sediment flux incision model described by *Whipple and Tucker* [2002] predicts that channel slopes can both rise and fall in response to a single increase in uplift rate, in contrast with detachment-limited stream power models that predict that slopes only increase in response to an increase in uplift rate.

[8] In this study we expand on the work of *Whipple and Tucker* [2002] and *Gasparini et al.* [2006] and explore two different bedrock incision models based on the studies by *Sklar and Dietrich* [2004] and *Parker* [2004]. Both of these models are formulated to capture the dual role that the bed load sediment flux plays in both enhancing incision through sediment impacts on the channel bed and hindering incision by covering the bed. The details of these models differ from the sediment-flux-dependent incision models considered by *Whipple and Tucker* [2002] and *Gasparini et al.* [2006]. Our focus remains solely on the role that the sediment flux carried as bed load plays on bedrock channel incision. We do not consider any other variables that likely play a role in bedrock channel evolution, such as bed roughness, channel width, or lithology; nor do we consider other processes that enhance bedrock incision, such as plucking or weathering.

[9] We explore the behavior of nonsteady state bedrock incision models using the CHILD numerical landscape evolution model [*Tucker et al.*, 2001a, 2001b]. CHILD models a number of different physical processes, but we include only three in our experiments: fluvial incision, rock uplift, and diffusion. The general equation that controls landscape evolution is

$$\frac{\partial z}{\partial t} = U - I - H, \tag{1}$$

where U is the rock uplift term (measured relative to a fixed base level), which is positive and uniform in space in all of our experiments; I is the fluvial incision term which we describe in detail in the following section; and H is the hillslope erosion rate. We model hillslope erosion as a diffusive process following many previous studies [e.g., *Kirkby*, 1986; *Willgoose et al.*, 1991; *Howard*, 1994; *Tucker and Bras*, 1998]:

$$H = k_d \nabla^2 z. \tag{2}$$

Equation (2) is appropriate for processes such as soil creep and rain splash on soil-mantled slopes. Our paper focuses on the competition between fluvial incision and rock uplift, however, we must include a hillslope component to supply headwater channels with the sediment that is needed to drive fluvial incision.

2. Incision Models

[10] This study focuses on the predicted steady state and transient behavior of sediment-flux-dependent bedrock incision models. We explore two models in detail, which are

derived from the models presented *Sklar and Dietrich* [2004] and *Parker* [2004]. Before describing the details of these models, we present the general form that these models and other proposed sediment flux bedrock incision models follow [*Beaumont et al.*, 1992; *Whipple and Tucker*, 2002; *Gasparini et al.*, 2006]:

$$I = Kf(Q_s)A^m S^n, \tag{3}$$

in which A is the drainage area; S is channel slope; $f(Q_s)$ is the sediment flux erodibility, which varies as a function of the sediment flux and sediment transport capacity; K is a parameter whose exact meaning varies between the models, but in general it varies with the strength of the bedrock (larger K implies less resistant lithologies) and climate (in the stream power model, larger K implies more erosive climatic conditions, however, this is not the case with either of the models presented in this paper); and m and n are dimensionless constants that vary between the different formulations that we present. The detachment-limited stream power model, which does not include the influence of sediment flux on bedrock incision, is simply equation (3) with $f(Q_s) = 1$.

[11] In equation (3), $A^m S^n$ is a stand-in for the shear stress term and the values of m and n indicate how the incision rate scales with bed shear stress for a constant value of $f(Q_s)$. (A derivation for shear stress as a function of A and S is given below.) There are no universal values of m and n. Generally, m and n are both positive, and their ratio (m/n) is considered to be $\approx$0.5, in which case $A^m S^n$ scales with shear stress to a positive power [*Tucker and Whipple*, 2002].

[12] For the two models considered here, the sediment flux erodibility, or $f(Q_s)$, is

$$f(Q_s) = \frac{Q_s}{W}\left(1 - \frac{Q_s}{Q_t}\right), \tag{4}$$

where Q_s is the incoming volumetric bed load sediment flux, Q_t is the volumetric bed load sediment transport capacity, and W is the channel width. Equation (4) only applies when $Q_s < Q_t$ and $f(Q_s) > 0$; when $Q_s > Q_t$ the channel becomes transport limited and equation (3) no longer applies. Throughout this study, equation (4) is always used to calculate the sediment flux erodibility term. Although the models that we discuss in this study differ in important details, they both follow the form of equation (3); only the values of K, m and n vary between the two models that we use.

[13] We assume that channel width is a function of the fluvial discharge:

$$W = k_w Q^b. \tag{5}$$

Although this relationship was originally observed in alluvial channels [*Leopold and Maddock*, 1953], recent studies support that the hydraulic geometry relationship also holds in many bedrock channels [e.g., *Montgomery and Gran*, 2001; *Snyder et al.*, 2003b; *Tomkin et al.*, 2003; *van der Beek and Bishop*, 2003; *Wohl*, 2004; *Finnegan et al.*, 2005]. In this study we always set $b = 1/2$.

[14] To calculate the sediment transport capacity, we simplify the general form that many sediment transport equations follow [e.g., *Meyer-Peter and Müller*, 1948; *Wilson*, 1966; *Fernandez Luque and van Beek*, 1976]:

$$Q_t \propto W(\tau - \tau_c)^{3/2} \tag{6}$$

where τ is the basal shear stress, and τ_c is the critical shear stress for entrainment of sediment, which is a function of the size of grains on the bed [e.g., *Shields*, 1936; *Komar and Li*, 1986; *Parker*, 1991; *Wilcock*, 1998]. Assuming uniform, steady flow in a wide channel and using the Darcy-Weisbach flow resistance equation, bed shear stress can be expressed as [e.g., *Tucker and Slingerland*, 1996],

$$\tau = \frac{\rho g^{2/3} f^{1/3}}{2}\left(\frac{Q}{W}\right)^{2/3} S^{2/3}, \tag{7}$$

where g is the acceleration of gravity, ρ is the water density, and f is a dimensionless roughness parameter. Fluvial discharge is expressed as a function of drainage area:

$$Q = k_q A^c \tag{8}$$

where $c \leq 1$ and k_q is related to the effective precipitation rate and the hydrology of the watershed [e.g., *Slingerland et al.*, 1994; *O'Connor and Costa*, 2004; *Solyom and Tucker*, 2004]. Assuming $b = 1/2$ and $c = 1$, equation (7) becomes

$$\tau = k_\tau A^{1/3} S^{2/3}, \tag{9}$$

where

$$k_\tau = \frac{\rho g^{2/3} f^{1/3} (k_q)^{1/3}}{2(k_w)^{2/3}} \tag{10}$$

Combining equations (6) and (9), the sediment transport capacity can be written as

$$Q_t \propto k_w A^{1/2}\left(k_\tau A^{1/3} S^{2/3} - \tau_c\right)^{3/2}. \tag{11}$$

We simplify this equation by dropping the threshold term, which leads to $Q_t \propto A^1 S^1$ or in general,

$$Q_t = K_t A^{m_t} S^{n_t}, \tag{12}$$

[*Willgoose et al.*, 1991; *Tucker and Slingerland*, 1997; *Whipple and Tucker*, 2002]. By making this simplification, the parameter K_t is not directly related to physical constants. However K_t still has the same sensitivity to parameters as k_τ, implying that K_t increases with the erosive power of the climate. This expression for sediment transport capacity is common to all models in this study and that of *Gasparini et al.* [2006]. Note that m_t and n_t are not the same as the exponents m and n in equation (3).

[15] Because we drop the threshold term in the sediment transport capacity relationship, we cannot directly model the influence of bed load grain size variation (these effects are

also ignored in the derivation of the bedrock incision models given below). Without the threshold term, it easier to predict and model channel behavior, however, the threshold has important influences on channel concavity [e.g., *Snow and Slingerland*, 1987; *Sinha and Parker*, 1996; *Morris and Williams*, 1997; *Gasparini et al.*, 2004]. The effect of a threshold on channel concavity can be mimicked by increasing the value for m_t and appropriately adjusting K_t, as first proposed by *Howard* [1980]. In all of the following analytical derivations, we assume that $n_t = 1$ (consistent with equation (11)), but we do not fix the value of m_t. However, in all of our simulations, we set $m_t = 1.5$.

[16] The variable Q_s is the volume of material eroded upstream of a point that is carried as bed load over a given time (or a single time step in CHILD). Q_s is a function of the erosion rate on both the hillslopes and the upstream channels. Any material removed through bedrock incision is transported downstream (assuming a sufficient transport capacity) and contributes to the sediment flux in the downstream nodes. Any material removed through hillslope erosion is eventually transported off the hillslope and into the channel, also becoming part of the sediment flux. In the numerical experiments, sediment is routed downstream and the total incoming sediment load is calculated at each point in the landscape.

[17] At steady state, the erosion rate is balanced by the uplift rate at every location in the landscape. It follows that the amount of material fluxing through any point is simply the product of the rock uplift rate (assuming uniform uplift) and the upstream drainage area. Given these conditions, the steady state bed load sediment flux ($\mathbf{Q_s}$) must be described as:

$$\mathbf{Q_s} = \beta U A, \tag{13}$$

where β is the fraction of eroded material that contributes to the bed load. Equation (13) is not contained in the CHILD numerical model; it is used solely to derive the analytical solutions for channel steady state behavior. Throughout this paper, bold variables indicate predicted or analytically derived steady state values. Steady state expressions are not explicitly contained in the CHILD numerical model.

[18] Combining the generic incision equation (3) with the equations for the sediment flux erodibility (4), channel width (5), sediment transport capacity (12) and steady state sediment flux (13), results in the following general expression for the steady state incision rate ($\mathbf{I}$):

$$\mathbf{I} = \beta U \frac{K}{k_w k_q^{1/2}} \left(A^{1/2+m} S^n - \frac{\beta U}{K_t} A^{3/2+m-m_t} S^{n-n_t} \right). \tag{14}$$

Equation (14) applies only at steady state, whereas equation (3) applies at all times and is the actual equation contained in the CHILD model.

2.1. Saltation-Abrasion Model

[19] The saltation-abrasion model presented here is a close approximation to the model presented by *Sklar and Dietrich* [1998, 2001, 2004]. The Sklar-Dietrich model is presently the most fully developed process-specific bedrock incision model for abrasion by saltation of a single grain size on a planar bed. Their formulation expresses bedrock incision as the product of three measurable terms which combine into

$$I_{SA} = \left[\frac{(w_{si})^2}{2\varepsilon_v} \right] \left[\frac{Q_s}{W L_s} \right] \left[1 - \frac{Q_s}{Q_t} \right]. \tag{15}$$

The first bracketed term represents the average volume of rock detached per particle impact, which is proportional to the ratio of the square of the vertical component of particle velocity at the bed (w_{si}) to the rock resistance to abrasion (ε_v). The second bracketed term represents the rate of particle impacts, which varies directly with the sediment flux per unit width ($\frac{Q_s}{W}$) and inversely with the particle saltation hop length, L_s. The third bracketed term represents the fraction of exposed bedrock on the channel bed; as the ratio of sediment flux to transport capacity ($\frac{Q_s}{Q_t}$) increases, less of the channel bed is exposed and vulnerable to abrasion. Downstream variations in grain size affect the values of w_{si}, L_s, and Q_t, but these variations have yet to be considered directly in the model.

[20] Using the geometry of particle saltation hops over a planar bed, *Sklar and Dietrich* [2004] express w_{si} as,

$$w_{si} = \frac{3 H_s u_s}{L_s}, \tag{16}$$

where H_s is the saltation height, and u_s is the average horizontal component of particle velocity. *Sklar and Dietrich* [2004] analyzed experimental observations of H_s, u_s and L_s as a function of particle diameter (D), submerged specific gravity (R_b), and transport stage (τ^*/τ_c^*, where τ^* is Shield's stress and τ_c^* is the critical Shield's stress) and found that equation (15) could be rewritten as:

$$I_{SA} = \frac{R_b g}{25 \varepsilon_v} \left(\frac{\tau^*}{\tau_c^*} - 1 \right)^{-0.52} \frac{Q_s}{W} \left(1 - \frac{Q_s}{Q_t} \right), \tag{17}$$

for $1 < \frac{\tau^*}{\tau_c^*} < 10$ (the range in which the Shield's stress is below the threshold for suspension of sediment). The negative exponent (-0.52) on excess transport stage reflects the fact that saltation length increases much more rapidly with τ^* than does the vertical component of particle impact velocity.

[21] With only a minor approximation, equation (17) can be expressed in the form of our generic sediment flux incision model (equation (3)). Linear regression analysis shows that the excess transport stage term can be reasonably well approximated by a simpler form:

$$\left(\frac{\tau^*}{\tau_c^*} - 1 \right)^{-0.52} \approx 2 \left(\frac{\tau^*}{\tau_c^*} \right)^{-0.88} \approx 2 \left(\frac{\tau}{\tau_c} \right)^{-0.88} \tag{18}$$

Using this approximation, the Sklar-Dietrich model can be recast approximately as,

$$I_{SA} = \frac{2 R_b g (\tau_c)^{0.88}}{25 \varepsilon_v} \frac{Q_s}{W} \left(1 - \frac{Q_s}{Q_t} \right) \tau^{-0.88}. \tag{19}$$

Finally, we substitute the expression for shear stress as a function of drainage area and slope (equation (9)) into equation (19) and approximate the shear stress exponent as $-3/4$ (as opposed to -0.88), to define the saltation-abrasion model (SA), or modified Sklar-Dietrich model:

$$I_{SA} = K_{SA}\frac{Q_s}{W}\left(1-\frac{Q_s}{Q_t}\right)A^{-1/4}S^{-1/2}, \tag{20}$$

where

$$K_{SA} = \frac{2R_b g}{25\varepsilon_v}\left(\frac{\tau_c}{k_\tau}\right)^{3/4}. \tag{21}$$

We make the approximation that $I_{SA} \propto \tau^{-3/4}$ in order to derive analytical solutions for the steady state and transient channel slope and threshold drainage area. These expressions provide a deeper understanding of the model behavior while still retaining most of the characteristics and sensitivities of the full saltation-abrasion model of *Sklar and Dietrich* [2004]. Note that equation (20) has the exact form as the general incision equation (equation (3)), with $m = -1/4$, $n = -1/2$, and K described by equation (21). The sediment transport capacity (Q_t) is calculated using equation (12).

[22] In contrast with the stream power model, for a fixed value of the sediment flux erodibility ($f(Q_s)$), bedrock incision rates decline as shear stress increases (negative m and n values in equation (20)). Because of the inverse relationship between incision rate and bed shear stress, K_{SA} decreases with increasing precipitation rate.

[23] Steady state is reached when the bedrock incision rate matches the uplift rate throughout the landscape. Making the assumptions of uniform uplift, $b = 1/2$, $c = 1$ and $n_t = 1$, and substituting the equations for channel width (5), sediment transport capacity (12), and steady state sediment load (13) into the saltation-abrasion model above (20), we find the following expression for the steady state saltation-abrasion incision rate:

$$\mathbf{I_{SA}} = U = \beta U K_{SA}\left(A^{1/4}S^{-1/2} - \frac{\beta U}{K_t}A^{5/4-m_t}S^{-3/2}\right). \tag{22}$$

Equation (22) can be written in a cubic form by rearranging and substituting $x = S^{-1/2}$:

$$x^3 - (\mathbf{S_{TL}})^{-1}x = -\left(\mathbf{S_{TL}}K_{SA}\beta A^{1/4}\right)^{-1}. \tag{23}$$

$\mathbf{S_{TL}}$ is the steady state slope under transport-limited conditions [*Whipple and Tucker*, 2002]:

$$\mathbf{S_{TL}} = \left(\frac{\beta U}{K_t}\right)A^{1-m_t}. \tag{24}$$

Equation (23) is a cubic and thus has three roots. Here we describe only some of the steady state solution space, but a more detailed explanation of the solutions to equation (23) is given by *Crosby et al.* [2007].

[24] The right-hand side of equation (23) approaches zero when either K_{SA} is relatively large (weak rock, smaller discharge), or A is large. Under either of these conditions, $x = (\mathbf{S_{TL}})^{-1/2}$, or equivalently, the steady state slope is the transport slope. In all cases, at large drainage areas the steady state saltation-abrasion slope converges to the transport slope. Under these conditions, erosion rate converges on the divergence of sediment flux as expected for transport-limited conditions.

[25] When K_{SA} and A are not large, a general solution of equation (23) [see *Crosby et al.*, 2007] predicts the steady state slope for the saltation-abrasion model ($\mathbf{S_{SA}}$):

$$\mathbf{S_{SA}} = \left[1.15(\mathbf{S_{TL}})^{-1/2} \cdot \cos\left(\frac{\cos^{-1}\left(-2.60\left(K_{SA}\beta A^{1/4}\right)^{-1}(\mathbf{S_{TL}})^{1/2}\right)}{3}\right)\right]^{-2}. \tag{25}$$

The $\cos^{-1}$ function is only defined for values in the range $[-1, 1]$. The limited solution space of equation (25) defines a critical drainage area ($\mathbf{A_{SA_c}}$) below which there is no real solution to equation (25). The critical drainage area is reached when $2.60\,(K_{SA}\beta A^{1/4})^{-1}(\mathbf{S_{TL}})^{1/2} = 1$, resulting in the following expression:

$$\mathbf{A_{SA_c}} = \left(\frac{27U}{4\beta K_t (K_{SA})^2}\right)^{\frac{1}{m_t-1/2}}. \tag{26}$$

When $A < \mathbf{A_{SAc}}$, the sediment supply is too small for the incision rate to keep pace with the uplift rate, and slopes predicted by equation (25) become infinitely steep, implying either the spontaneous formation of waterfalls, or that other processes become important and limit channel slope. Drainage areas which are smaller than the critical drainage area are tools-starved.

[26] The steady state slope-area relationship predicted by the saltation-abrasion model is illustrated in Figure 1. Steady state slopes grow infinitely large as they approach the critical drainage area. The critical drainage area increases with uplift rate (see equation (26) and compare the solid line with the dash-dotted line in Figure 1). As a result, drainage density decreases with increasing incision rate. The critical drainage area also increases as K_{SA} decreases. Stronger rocks require more tools for wear, and therefore a larger contributing area is needed to supply these tools.

[27] Similarly to other incision models, the saltation-abrasion model also predicts that steady state slopes increase with uplift rate [e.g., *Whipple and Tucker*, 1999] (all else being equal; compare the solid line with the dash-dotted line in the slope plot in Figure 1). An increase in bedrock strength (decrease in K_{SA}) results in steeper slopes in part of the reach; however, because the slopes converge to transport-limited conditions at large drainage areas, a change in rock strength makes no difference at large drainage areas (compare the solid line with the dashed line in Figure 1, top).

[28] Changes in $f(Q_s)$ with U and K_{SA} are also illustrated in Figure 1. Although variation in K_{SA} does not affect the steady state slope at large drainage areas, variation in K_{SA} does affect the value of $f(Q_s)$. More resistant rock, or smaller K_{SA}, requires a larger value of $f(Q_s)$ in order to incise at the same rate as weaker rock (compare the dashed

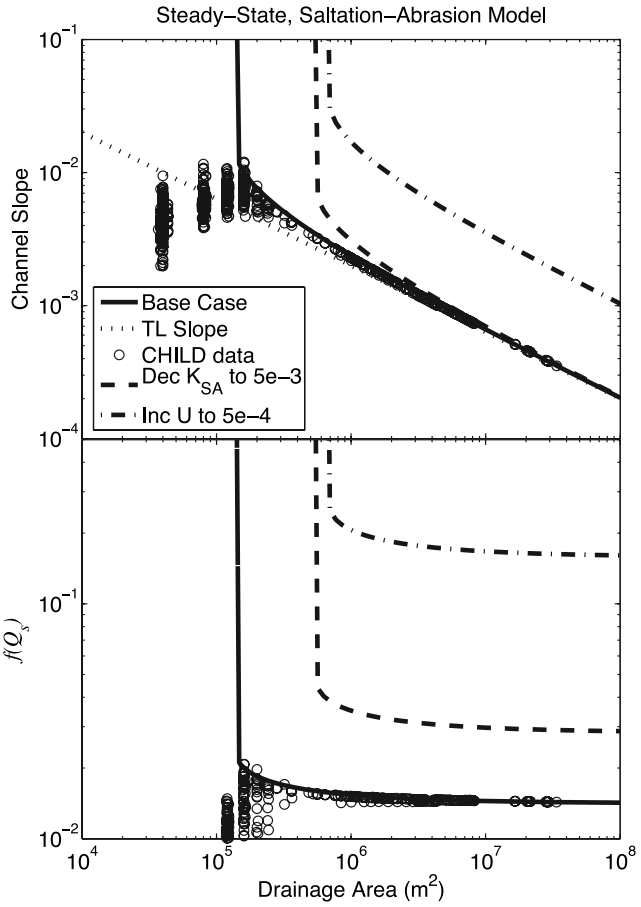

Figure 1. Predicted steady state slope-area and $f(Q_s)$-area relationships using the saltation-abrasion model (solid line), transport-limited model (dotted line, slope-area plot only), and results from a numerical experiment using CHILD (circles). (Base parameter values are $m = -0.25$, $n = -0.5$, $K_{SA} = 1 \times 10^{-2}$ m$^{-0.5}$, $m_t = 1.5$, $n_t = 1$, $K_t = 5 \times 10^{-5}$ yr^{-1}, $k_d = 5$ m^2/yr, and $U = 1 \times 10^{-4}$ m/yr.) The dashed line shows how the saltation-abrasion solution varies if only K_{SA} is decreased. The dashed-dotted line shows how the saltation-abrasion solution varies if only the uplift rate is increased. In both plots the predicted relationships are plotted as a vertical line at the critical drainage area (equation (26)).

line with the solid line in Figure 1, bottom). $f(Q_s)$ also increases with uplift rate, leading to higher incision rates (compare the solid line with the dash-dotted line in Figure 1, bottom). Note that changes in $f(Q_s)$ imply adjustments in the fraction of bedrock exposed on the channel floor (see discussion by *Sklar and Dietrich* [2004]). The circles in Figure 1 (bottom) (illustrating the CHILD data) show that below $\mathbf{A_{SA_c}}$, the landscape is experiencing some fluvial erosion, but this region is dominated by hillslope erosion.

[29] The CHILD slope-area data (circles in Figure 1, top) conform closely to the analytical steady state solution (equation (25)). In the region in which slopes are no longer defined by the saltation-abrasion model ($A < \mathbf{A_{SA_c}}$), hillslope processes dominate erosion (equation (2)). The hillslope region is always recognizable as the region in which, on average, slopes increase with drainage area [e.g., *Tucker and Bras*, 1998]. The landscape transitions from hillslope dominated processes to fluvial processes where the diffusive slope-area solution intersects the fluvial slope-area solution [*Tucker and Bras*, 1998]. By setting the diffusivity coefficient (k_d) larger or smaller, we can force this transition to occur at larger or smaller drainage areas, respectively. Arrows in Figure 2 indicate the slope at the transition from hillslope to fluvial channel for different values of k_d.

[30] In each of our simulations, we choose the hillslope diffusivity coefficient so that the landscape transitions from hillslope to channel at an area as close to the critical area as possible. Although somewhat arbitrary, we must do this in order to illustrate the unique behavior of the abrasion models. However, we recognize that in landscapes where k_d is large, and hillslope lengths are long, the region of the landscape near the critical drainage area could be dominated by hillslope processes, and therefore the unique behavior of the channel near the critical area could be masked (see the dashed line and arrow in Figure 2). Similarly, if k_d is too small, the model would produce large, and in many cases unrealistic, slope discontinuities near the critical drainage area (dotted line and arrow in Figure 2). In the example with $k_d = 0.5$ in Figure 2, slopes would drop from a gradient of $\approx$0.07 to $\approx$0.01 at the transition from hillslope to channel. This slope discontinuity might not occur in natural land-

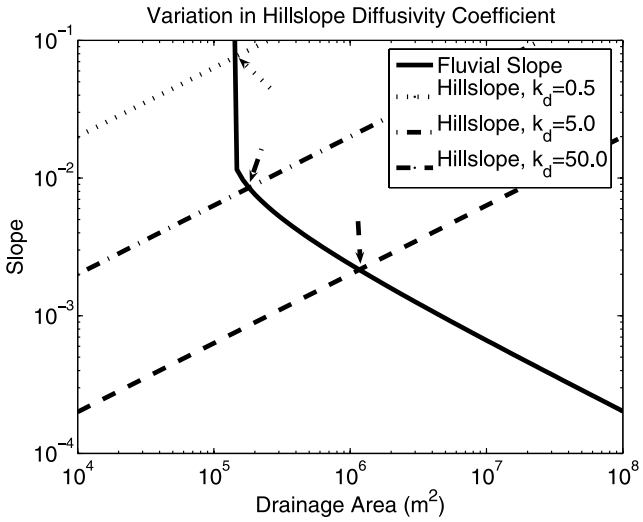

Figure 2. Effect, in steady state, of varying k_d while keeping the fluvial parameters fixed at the values used for the base example in Figure 1. The arrows point out the transition in slope-area space from hillslope (dashed, dash-dotted, and dotted lines) to fluvial channel (solid line). The dash-dotted line illustrates the hillslope diffusivity used in the CHILD example illustrated in Figure 1. A larger k_d (dashed line) leads to longer hillslopes and transition from hillslope to channel at a larger drainage area and a shallower slope. Similarly, a smaller k_d (dotted line) leads to shorter hillslopes and a transition from hillslope to channel at a smaller drainage area. The smallest k_d example includes an abrupt discontinuity in slope at the transition owing to the instability of both sediment-flux-dependent incision models at low-drainage areas (see equations (26) and (31) for the critical drainage area using the saltation-abrasion and generalized abrasion models, respectively).

scapes because other processes not included in the numerical model, such as debris flows, weathering or plucking, could reduce slopes in this region.

2.2. Generalized Abrasion Model

[31] *Parker* [2004] presents a model for incision into bedrock that includes two processes: wear by saltating bed load and plucking of bedrock blocks. In this study we consider only the formulation for wear by saltating bed load, which is very similar to the Sklar-Dietrich model but does not account for single grain size saltation dynamics over a planar bed. Parker's abrasion module is the product of two terms, one representing the volume of material detached as particles impact the bed through saltation and the second representing particle shielding of the bed from grain collisions. Parker's abrasion module follows exactly the same form as the general incision model we presented earlier (equation (3)) with $m = n = 0$:

$$I_{GA} = K_{GA}\frac{Q_s}{W}\left(1 - \frac{Q_s}{Q_t}\right), \tag{27}$$

where

$$K_{GA} = \frac{r}{L_s}. \tag{28}$$

r is the fraction of the particle volume detached off the bed with each particle collision. K_{GA} is not a function of climate, but, similarly to other bedrock incision models, a larger K_{GA} implies more bedrock is detached per particle impact, and therefore the rock is weaker. Because $m = n = 0$, incision rates predicted by the generalized abrasion model do not vary with bed shear stress when $f(Q_s)$ is fixed. Although equation (27) does not contain the $A^m S^n$ term that the reader may be accustomed to seeing, we remind the reader that the sediment transport capacity, Q_t, that appears in the above equation, is a function of drainage area and slope (see equation (12)).

[32] The primary difference between the Parker model and the Sklar-Dietrich model is that *Parker* [2004] considers the saltation hop length (L_s) to be constant, while *Sklar and Dietrich* [2004] express the saltation hop length as a function of transport stage. Equation (27) is identical to the *Parker* [2004] abrasion module. The only difference between Parker's abrasion module and the generalized abrasion model that we implement in CHILD is that we use a simpler formulation for the sediment transport capacity (Q_t, equation (12)). *Parker* [2004] considers a threshold for sediment transport, while we ignore thresholds in order to derive analytical steady and nonsteady solutions to predict model behavior.

[33] The steady state generalized abrasion incision equation in a landscape with uniform uplift is described by assuming $b = 1/2$, $c = 1$, $n_t = 1$, and combining the equations for channel width (5), sediment transport capacity (12) and steady state sediment load (13) with the incision equation above (27):

$$\mathbf{I_{GA}} = U = \beta U K_{GA}\left(A^{1/2} - \frac{\beta U}{K_t}A^{3/2-m_t}S^{-1}\right) \tag{29}$$

This equation can be rearranged to find the steady state slope-area relationship:

$$\mathbf{S_{GA}} = \left(\frac{\beta U}{K_t}A^{1-m_t}\right)\left(1 - \frac{1}{\beta K_{GA}}A^{-1/2}\right)^{-1}. \tag{30}$$

The leading term in equation (30) is the transport-limited slope (equation (24)). Similarly to the saltation-abrasion model, the generalized abrasion model converges to the transport slope at large drainage areas. At small drainage areas, predicted slopes are infinite because the sediment flux is too small to produce wear rates that keep pace with the uplift rate. The critical drainage area below which there is no solution to the generalized abrasion model is

$$\mathbf{A_{GA_c}} = (\beta K_{GA})^{-2}. \tag{31}$$

Smaller values of K_{GA} (strong rock) increase the critical drainage area. Unlike the saltation-abrasion model, the critical drainage area for the generalized abrasion model does not vary with rock uplift rate.

[34] The sensitivity of steady state slopes to K_{GA} is illustrated by the solid and dashed lines in Figure 3 (top). A smaller K_{GA} (dashed line) leads to a larger critical drainage area and a smaller drainage density. However, at larger drainage areas both of these solutions converge to the same transport-limited solution and the value of K_{GA} no longer plays a role in setting the steady state slope (dotted line in Figure 3, top). The example with the larger value of K_{GA} (solid line) converges to transport-limited conditions at a smaller drainage area; a larger value of K_{GA} implies more easily erodible rock, which is likely to reach transport-limited conditions at a smaller drainage area.

[35] Figure 3 also illustrates the differences in the steady state slope between low uplift (solid line) and high uplift (dash-dotted line) conditions. The critical drainage area does not vary with uplift (equation (31) does not contain U). For a given area (greater than the critical drainage area), steady state slopes increase with rock uplift rate, similar to the behavior of the detachment-limited stream power model and other models that incorporate sediment flux [*Whipple and Tucker*, 1999; *Snyder et al.*, 2000; *Gasparini et al.*, 2006].

[36] The sensitivity of steady state $f(Q_s)$ values to K_{GA} and U is also illustrated in Figure 3. All else being equal, a more resistant rock has a larger value of $f(Q_s)$ (compare the dashed line (more resistant) with the solid line (less resistant)). In more resistant rock the sediment essentially has to work harder to wear away at the bed, hence $f(Q_s)$ increases as K_{GA} decreases. $f(Q_s)$ increases with uplift rate, resulting in an increase in incision rates. Note that $f(Q_s)$ is the only term that can adjust to changes in incision rate with this model, because $m = n = 0$ in equation (3). Hence, for uniform rock uplift, $f(Q_s)$ is always constant across a steady state landscape, in contrast to the saltation-abrasion model which predicts that $f(Q_s)$ decreases downstream. The steady state bed cover predictions of these two models are, in principle, testable in the field.

[37] The CHILD data illustrated in Figure 3 are from a steady state landscape that transitions from hillslope-dominated to fluvially dominated processes in a region of

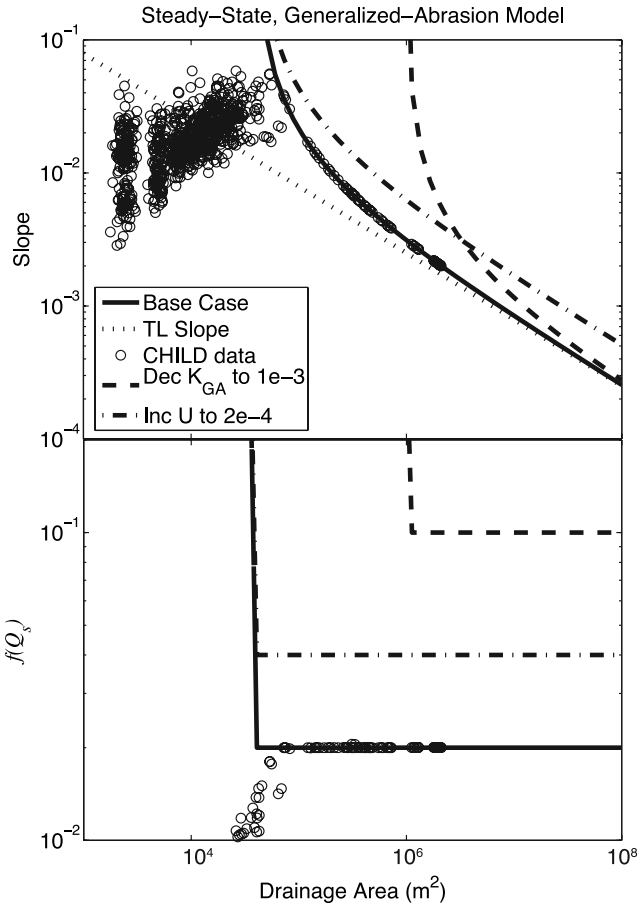

Figure 3. Predicted steady state slope-area and $f(Q_s)$-area relationships for the generalized abrasion model (solid line), transport-limited model (dotted line, slope-area plot only), and results from a numerical experiment using CHILD (circles). (Base parameter values are $m = 0.0$, $n = 0.0$, $K_{GA} = 5 \times 10^{-3}$ m^{-1}, $m_t = 1.5$, $n_t = 1$, $K_t = 4 \times 10^{-5}$ yr^{-1}, $k_d = 1$ m^2/yr, and $U = 1 \times 10^{-4}$ m/yr.) The dashed line shows how the generalized abrasion solution varies if only K_{GA} is decreased. The dashed-dotted line shows how the generalized abrasion solution varies if only the uplift rate is increased. In both plots the predicted relationships are plotted as a vertical line at the critical drainage area (equation (31)).

the generalized abrasion solution where slopes are rapidly decreasing with drainage area (local channel concavity is very large). Because the channel slopes are rapidly decreasing downstream and the channels are surrounded by steep hillslopes, the landscape has the appearance of having an incised valley near the channel head (Figure 4). The steep regions around the channel heads are unrealistic and appear as a consequence of not including certain processes in the numerical model that might dominate in this region, such as debris flows [*Stock and Dietrich*, 2003].

3. Main Channel Response to an Increase in Uplift Rate

[38] As discussed in the previous section, both sediment flux incision models behave in a similar manner at steady state (assuming uniform uplift). They approach transport-limited conditions at large drainage areas. Both models have a critical drainage area below which incision rates can no longer keep pace with uplift rates, although the controls on the critical drainage area vary between the two models. As in both the detachment-limited stream power model and the transport-limited model, both the saltation-abrasion and generalized abrasion models predict that steady state slopes increase with uplift rate. However, contrary to previously presented incision models and natural observations [e.g., *Tucker and Whipple*, 2002], both the saltation-abrasion and generalized abrasion models predict that channel concavity varies downstream. Downstream changes in bed load grain size, however, could counteract this tendency [*Sklar*, 2003].

[39] If the sediment flux models predict steady state behavior that is similar to that of transport-limited models in most of the landscape, the question arises as to whether or not the details of these models are important when addressing large-scale landscape evolution questions. To further explore the similarities among these models, we investigate the nonsteady state behavior of fluvial channels in response to an increase in uplift rate.

[40] Both the saltation-abrasion and the generalized abrasion models have a very small parameter space in which the critical drainage area is reasonably small and the channel does not converge to transport-limited conditions. The limited area over which these sediment-flux-dependent models apply and yet are distinct from the simple transport-limited models could be an indication that fluvial channels are only strictly abrasion dominated over a limited range of conditions, and other processes such as plucking, weathering, cavitation [*Whipple et al.*, 2000a] and debris flow scour [*Stock and Dietrich*, 2003] are required to fully model the dynamics of landscapes containing incising bedrock channels.

[41] We contrast the transient behavior of the network trunk stream to the behavior predicted in previous studies using various other incision models [*Whipple and Tucker*, 2002; *Gasparini et al.*, 2006]. *Crosby et al.* [2007] present a complementary analysis of tributary response to main stem incision. The ultimate goal of this study and others [*Whipple and Tucker*, 2002; *Gasparini et al.*, 2006; *Crosby et al.*, 2007] is to find diagnostic behavioral differences that can be exploited to critically and quantitatively evaluate competing river incision models against field data.

[42] The general landscape setting is the same for all of the experiments discussed, however the size and node spacing within the landscape varies between the experiments (Figure 4 illustrates an example landscape). All of the simulated landscapes are square with closed boundaries on all four sides which sediment and water cannot cross. Water and sediment can leave the network through one corner outlet that drains to a point with a fixed elevation of zero. Precipitation is uniform across the landscape and never changes. Erosion due to diffusive processes occurs at all points in the landscape, however it only contributes significantly at small drainage areas. Hillslope erosion supplies the channels with the sediment needed to initiate fluvial erosion. At drainage areas greater than A_c, fluvial incision is the dominant erosion process.

[43] All of the experiments are conducted in the same manner. A landscape is evolved to steady state using either

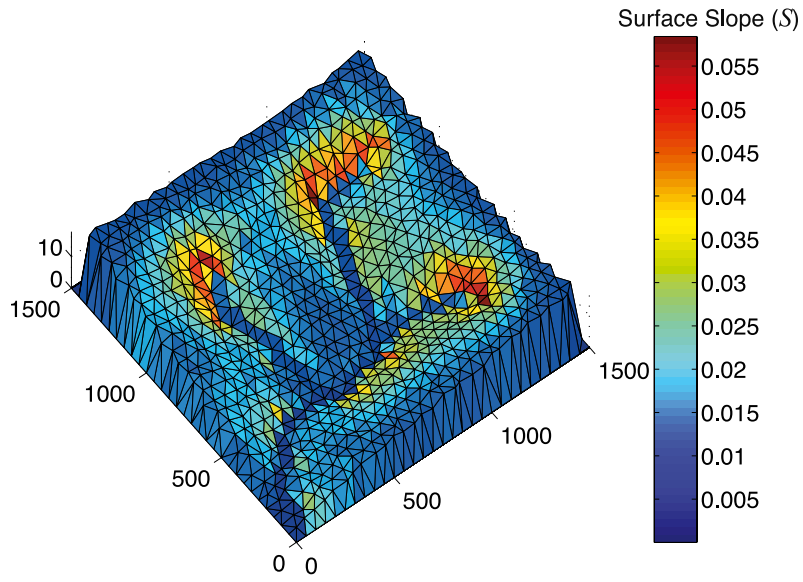

Figure 4. Steady state landscape produced using the generalized abrasion model with CHILD. Units on landscape axes are in meters. Landscape is shaded by the slope. (Parameter values are $m = 0.0$, $n = 0.0$, $K_{GA} = 5 \times 10^{-3}$ m^{-1}, $K_t = 4 \times 10^{-5}$ yr^{-1}, $k_d = 1$ m^2/yr, and $U = 1 \times 10^{-4}$ m/yr.) Figure 3 shows the slope-area and $f(Q_s)$ data from this landscape.

the saltation-abrasion or generalized abrasion model and a uniform uplift rate. Once steady state is reached, the uplift rate is instantaneously increased across the landscape. The outlet continues to drain to a point with a fixed elevation of zero. We investigate landscape response to this change in uplift rate, with emphasis on the transient evolution of the trunk channel in terms of both morphology (local slope, longitudinal profile form) and bed state (degree of alluvial cover, expressed as $f(Q_s)$ and $\frac{Q_s}{Q_t}$).

[44] In all cases that we illustrate the incoming sediment flux (Q_s) is less than the sediment transport capacity (Q_t) and bedrock incision controls channel evolution. However, if during the transient the incoming sediment flux were to surpass the sediment transport capacity, leading $f(Q_s) < 0$, the channel would deposit sediment and channel evolution would become transport limited [*Tucker et al.*, 2001a].

3.1. Transient Behavior Predicted by the Saltation-Abrasion Model

[45] Here we explore the predicted channel behavior in response to an increase in uplift rate using the saltation-abrasion model. Equation (20) is used to calculate the fluvial incision rate. We remind the reader that the sediment flux (Q_s) is a free variable, and the sediment transport capacity (Q_t, calculated using equation (12)) evolves with the channel slope. Because both Q_s and Q_t evolve through time, $f(Q_s)$ also varies throughout the numerical simulation.

[46] Under steady state conditions, equation (25) predicts that slopes are nearly linearly related to uplift rate. However, this equation does not apply when the network is responding to any type of perturbation. To facilitate discussion of the numerical results, we begin with an idealized analysis of initial channel response to an increase in uplift rate. As noted by *Whipple and Tucker* [2002], adjustments in the sediment load must lag behind initial changes in the channel slope. When the network first responds, slope is the sole variable adjusting to changes in uplift because the sediment flux initially remains the same. We can calculate the initial transient slope at any point by finding the slope that is needed to produce an incision rate equal to the new higher uplift rate with no change in sediment flux ($Q_s = \beta U_{old} A$, where U_{old} is the uplift rate prior to the increase). This assumption only holds during the initial response at any point in the network. At later times the sediment flux slowly increases to its new equilibrium value. The transient slope equation has a form similar to the steady state slope solution for the saltation-abrasion model (equation (25)). We do not include the transient slope equation here because it is difficult to infer slope behavior from the solution.

[47] We use the transient slope equation (not shown) to find an expression for the transient critical drainage area, below which fluvial slopes are predicted to be infinite:

$$A_{SA_{trans}} = \left(\frac{27\lambda^2 U_{old}}{4\beta K_t (K_{SA})^2} \right)^{\frac{1}{m_t - 1/2}}, \qquad (32)$$

where λ is the factor of increase in rock uplift rate ($\lambda = \frac{U_{new}}{U_{old}}$, where U_{new} is the rock uplift rate after the increase). The area at which the transient slope is no longer defined ($A_{SA_{trans}}$) is similar to the critical drainage area at steady state (equation (26)), and differs only by a factor $\lambda^{\frac{2}{m_t - 1/2}}$. The transient critical drainage area is always larger than the new steady state critical drainage area, which is larger than the original steady state critical drainage area (assuming an increase in rock uplift rate). This implies potentially unstable behavior during transient adjustments that are likely to lead to significant oversteepening of channel slopes in the part of the landscape near $A_{SA_{trans}}$. However, it is important to note that equation (32) is only strictly valid at the network outlet (effective value of λ will be reduced by attenuation as the uplift signal propagates upstream) and

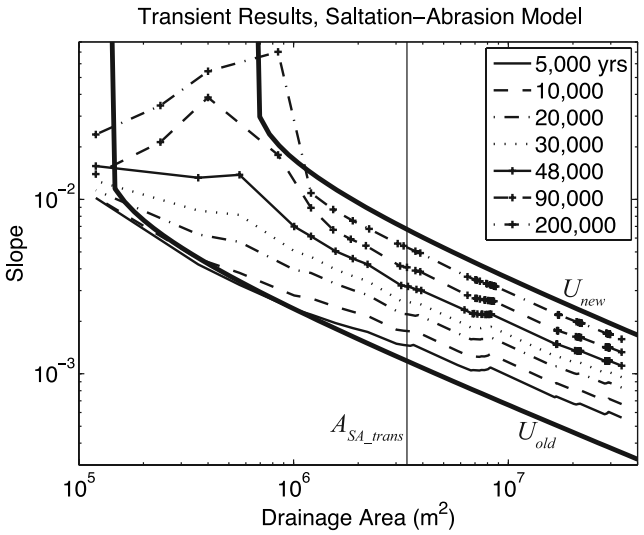

Figure 5. Changes in slope through time in response to a fivefold increase in uplift rate using the saltation-abrasion model. Step changes in slope, for example, at $A \approx 8 \times 10^6$ m^2, occur where large tributaries join the main stream. (Parameter values in this and Figures 6–9 are $m = -0.25$, $n = -0.5$, $K_{SA} = 1 \times 10^{-2}$ m$^{-0.5}$, $m_t = 1.5$, $n_t = 1$, $K_t = 5 \times 10^{-5}$ yr^{-1}, $k_d = 5$ m^2/yr, $U_{old} = 1 \times 10^{-4}$ m/yr, and $U_{new} = 5 \times 10^{-4}$ m/yr.) As a reference the predicted steady state slope-area relationships with the old and new uplift rates are shown, labeled U_{old} and U_{new}, respectively. The vertical line labeled $A_{SA_{trans}}$ demarcates the transient critical drainage area, predicted by equation (32). The total drainage area of the network is 3.6×10^7 m^2, and the node spacing is 200 m. Note that the time increments between the plotted lines change.

only at the first instant of network response, because at all later times $Q_s > \beta\, U_{old}\, A$. Thus the response of slopes near the transient critical area (equation (32)) may be dampened.

[48] Figures 5–9 illustrate the transient behavior in the main channel after an increase in uplift rate. The lower parts of the channel (large drainage areas) behave very similarly to a strictly transport-limited network where local erosion rate is governed by the divergence of sediment flux [*Whipple and Tucker*, 2002]. Slopes increase slowly in the large drainage area regions, and no large slope discontinuities or knickpoints are created (Figure 5), in contrast to predictions by the detachment-limited stream power model [*Whipple and Tucker*, 2002]. The steady state value of Q_s/Q_t decreases with an increase in uplift rate (less sediment cover on the bed), resulting in an increase in $f(Q_s)$ with uplift rate (Figures 7 and 8, respectively). The initial increase in slope in the lower reach of the main channel drives up the sediment transport capacity and causes Q_s/Q_t to decrease below its new equilibrium value (Figure 7). The decrease in Q_s/Q_t beyond its new steady state value during the transient does not cause $f(Q_s)$ to surpass its new steady state value (Figure 8). $f(Q_s)$ is not linearly related to Q_s/Q_t (equation (4)), and the changes in both Q_s and Q_t result in a steady increase in $f(Q_s)$ during the transient.

[49] In this example, the critical drainage area ($\mathbf{A_{SA_c}}$) for the new uplift rate is 6.75×10^5 m^2, and the predicted transient critical drainage area ($A_{SA_{trans}}$) is 3.4×10^6 m^2. The area at which slopes start to greatly steepen is approximately 9×10^5 m^2, which is less than the predicted transient critical drainage area (see vertical line in Figure 5) but larger than the predicted new steady state critical drainage area. The derivation for $A_{SA_{trans}}$ (equation (32)) assumes that the upper reaches of the network have not responded to the change in uplift rate and that the change in incision rate at a point is instantaneous. The actual area at which slopes greatly steepen is upstream of the predicted area because the uplift/incision signal is dampened as it propagates slowly upstream (Figure 9) due to the diffusive, approximately transport-limited initial response in the lower parts of the network.

[50] In the region where the slope oversteepens above its predicted new steady state value ($A \approx 9 \times 10^5$ m^2, final time step illustrated in Figure 5), the incision rate stops increasing and actually decreases slightly (final time step illustrated in Figure 9). In this region Q_s/Q_t is still declining (the bed has less sediment cover), and $f(Q_s)$ is still increasing (final time step illustrated in Figures 7 and 8, respectively), even while the incision rate declines. An increase in $f(Q_s)$ alone would drive up the incision rate ($I_{SA} \propto f(Q_s)\, A^{-1/4}\, S^{-1/2}$). Even though $f(Q_s)$ is increasing, the $S^{-1/2}$ term dominates when the slope over-steepens, and the incision rate decreases slightly. The slopes become so steep that the sediment has minimal contact with the bed, and the incision rate declines. At this point, the signal from the change in uplift is greatly dampened upstream (Figure 9). The upstream catchment slowly responds by sending more sediment downstream, and eventually incision rates begin to increase again. During this period, changes in fluvial incision are limited by the response of the upper tips of

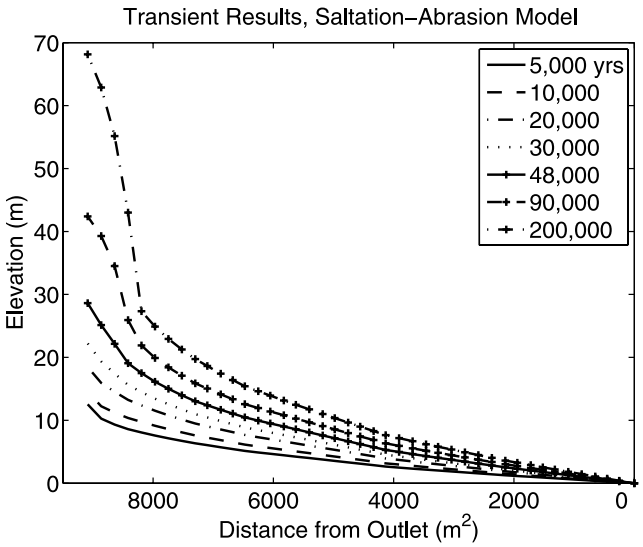

Figure 6. Changes in channel profile through time in response to a fivefold increase in uplift rate using the saltation-abrasion model. The slope along the profiles shown is illustrated in Figure 5. Note that the time increments between the individual profiles changes. Channel elevations are relative to the point which the network drains to that has a fixed elevation of zero.

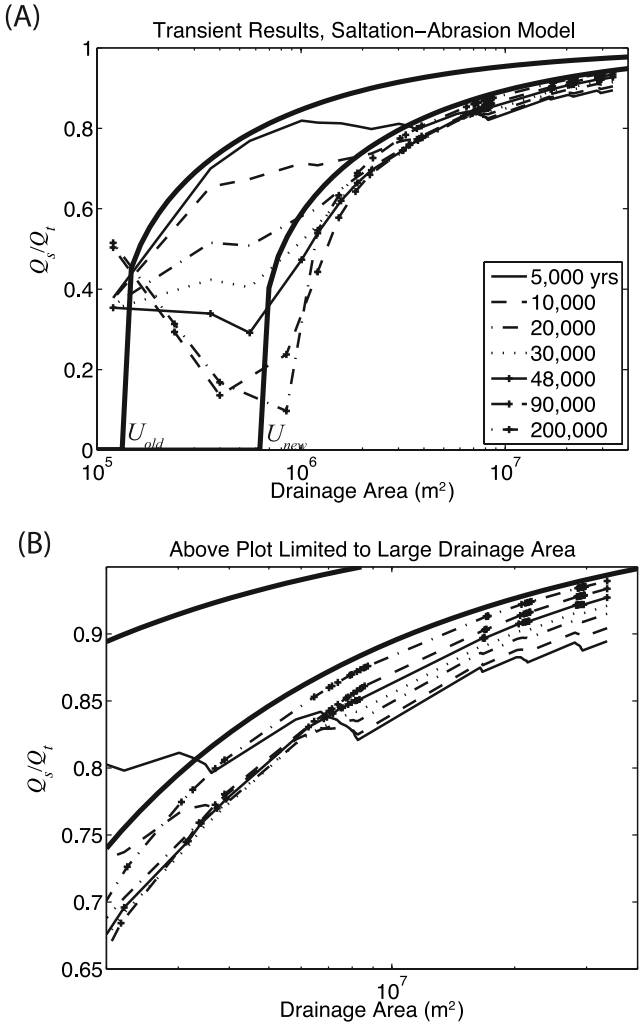

Figure 7. (a) Changes in the ratio of sediment flux to sediment carrying capacity through time in response to a fivefold increase in uplift rate using the saltation-abrasion model. (b) Closer view of the data at large drainage areas to show the details of the evolution. Step changes in Q_s/Q_t, especially visible at 5000 years, occur where large tributaries join the main stream. As a reference the predicted steady state Q_s/Q_t-area relationships with the old and new uplift rates are shown, labeled U_{old} and U_{new}, respectively. The channel slope-area relationships and channel profiles are shown in Figures 5 and 6. Note that the time increments between the individual lines change.

the river network and and the adjacent hillslopes. If not for the response of the upper catchment, channel slopes would be expected to increase without bound, eventually producing a waterfall.

[51] Because the steady state critical drainage area increases with uplift rate, the drainage density decreases with uplift rate. In the last two times illustrated in Figure 6, the upper parts of the main channel that were previously concave and controlled by fluvial process become convex, as diffusive processes take over. The time that it takes the upper catchment, including the hillslopes, to respond is critical to the downstream fluvial response with this model. If headwater catchments and hillslopes respond very slowly, this will increase the time during which slope instabilities such as the one illustrated in Figure 5 can grow. Including nonlinear diffusion or mass wasting processes would reduce hillslope response time [e.g., *Roering et al.*, 2001] and thus decrease the likelihood of downstream fluvial instabilities.

[52] Even though the location of oversteepening is very close to the new steady state critical drainage area, the oversteepening is truly part of the transient fluvial response. The oversteepened point is not destined to become hillslope once the new steady state is reached; rather, the oversteepening is driven by the dynamics of the saltation-abrasion model. We have performed a number of numerical experiments using the saltation-abrasion model with stronger perturbations in uplift rate and with different parameters. In some of these experiments the region of oversteepening is well downstream from the new steady state critical drainage area. In all cases, once a location starts to oversteepen, the incision rate declines. This acts as a positive feedback for the oversteepening because as the rate of increase in incision rates at upstream points slows down, so too does the increase in sediment flux. However, if and when hillslope response progresses sufficiently and the sediment flux increases to the point at which the incision can start to increase again, the oversteepened zone will begin to attenuate and propagate up the channel.

3.2. Transient Behavior Predicted by the Generalized Abrasion Model

[53] Here we explore the nonsteady state behavior of the generalized abrasion model. Equation (27) is used to calcu-

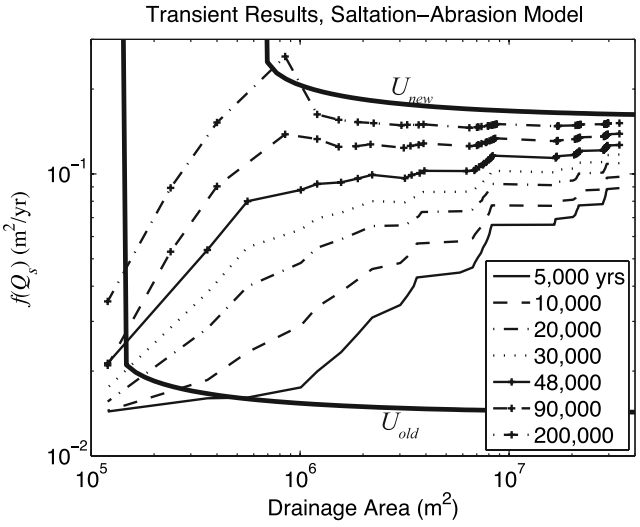

Figure 8. Changes in the sediment flux erodibility through time in response to a fivefold increase in uplift rate using the saltation-abrasion model. Step changes in $f(Q_s)$ occur where large tributaries join the main channel. As a reference the predicted steady state $f(Q_s)$-area relationships with the old and new uplift rates are shown, labeled U_{old} and U_{new}, respectively. The corresponding channel slope-area relationships, channel profiles, and Q_s/Q_t-area relationships are shown in Figures 5–7. Note that the time increments between the individual lines change.

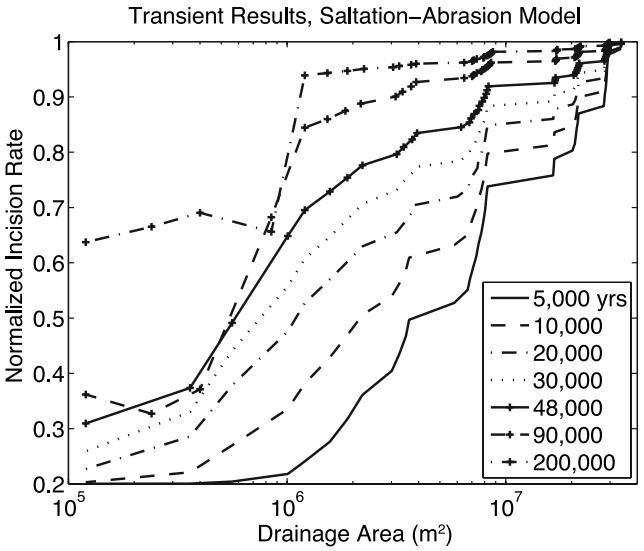

Figure 9. Changes in the incision rate normalized by the new uplift rate (values are dimensionless) using the saltation-abrasion model. The incision rate is averaged over a few thousand years and is not the instantaneous incision rate corresponding to the slope and $f(Q_s)$ values in Figures 5 and 8. Step changes in incision rate occur where large tributaries join the main channel. Note that the time increments between the individual lines change.

late the incision rate. We remind the reader that the sediment flux (Q_s) is a free variable, and the sediment transport capacity (Q_t, calculated using equation (12)) evolves with the channel slope. Because both Q_s and Q_t evolve through time, $f(Q_s)$ also varies throughout the numerical simulation.

[54] As we did with the saltation-abrasion model, we can assume that changes in sediment flux will lag changes in channel slope. If we make the assumption that the sediment flux does not change ($Q_s = \beta\ U_{old} A$) and that initially changes in slope alone drive up the incision rate, we can predict the transient channel slope:

$$S_{GA_{trans}} = \left(\frac{\beta U_{old}}{K_t}\right) A^{1-m_t} \left(1 - (\beta K_{GA})^{-1} \frac{U_{new}}{U_{old}} A^{-1/2}\right)^{-1}. \quad (33)$$

Again this relationship, and those derived from it, only strictly hold at the outlet and at the first instant of the transient response. We anticipate the simulated landscape to exhibit less extreme behavior than predicted by equation (33).

[55] The critical drainage area below which transient slopes become unstable (when the second bracketed term in equation (33) approaches zero) is given by

$$A_{GA_{trans}} = \left(\frac{\lambda}{\beta K_{GA}}\right)^2. \quad (34)$$

As was the case with the steady state solution, smaller values of K_{GA} (more resistant rock) cause slopes to become unstable at larger drainage areas. Further, larger increases in uplift rate (larger λ) result in slopes oversteepening at larger drainage areas. In contrast with the saltation-abrasion model, the transient critical drainage area predicted by the generalized abrasion model is not a function of the old uplift rate.

[56] We are also able to predict the area at which transient slopes are predicted to steepen above their new equilibrium value. (We were not able to derive this value using the saltation-abrasion model.) First we find an expression for the ratio of the transient slope to the new equilibrium slope:

$$\left(\frac{S_{GA_{trans}}}{\mathbf{S_{new}}}\right) = \lambda \left(\frac{1 - (\beta K_{GA})^{-1} A^{-1/2}}{1 - (\beta K_{GA})^{-1} \lambda A^{-1/2}}\right). \quad (35)$$

When $\frac{S_{GA_{trans}}}{\mathbf{S_{new}}} > 1$ then the transient slope is predicted to oversteepen above the new equilibrium slope. The predicted area at which slopes overshoot ($A_{GA_{os}}$):

$$A_{GA_{os}} < \left(\frac{1+\lambda}{\beta K_{GA}}\right)^2. \quad (36)$$

Equation (36) is a function only of the factor of change in uplift rate, and not of the absolute values of the old or new uplift rates.

[57] We performed a number of experiments to test the sensitivity of the generalized abrasion model to the magnitude of change in uplift rate. Smaller increases in uplift rate, in which the area of oversteepened slopes is predicted to occur close to the transient critical drainage area, behave similarly to the transient saltation-abrasion example illustrated in the previous section, or the transient prediction using transport-limited models [*Whipple and Tucker*, 2002]. In some cases, small knickpoints may form in the lower reaches after the initial perturbation, but at later times the slope slowly increases (similar to the mixed channel response describe by *Whipple and Tucker* [2002] or the first example illustrated by *Gasparini et al.* [2006] using the almost-parabolic model).

[58] We contrast the more gradual transient behavior predicted by the saltation-abrasion model with a more extreme example of transient behavior using the generalized abrasion model. We illustrate an example in which the uplift rate is increased by a factor of 10. Not only does equation (36) predict that the slope at the outlet will oversteepen, but also equation (34) predicts that the outlet slope will become infinite. The response of the main channel slopes and profiles is illustrated in Figures 10 and 11. The slope at the outlet quickly steepens beyond the new equilibrium value, creating a sharp discontinuity at the outlet. Figure 12 contrasts the initial topography with the topography after 20,000 years. Initially, elevation increases across the landscape because of the large increase in uplift rate (Figure 11, top), but the slopes change more slowly as the perturbation propagates up the channel (Figure 10, top). If this network was feeding into a larger channel, it might appear as a hanging tributary (see examples by *Crosby et al.* [2007]).

[59] During the transient period, the value of $\frac{Q_s}{Q_t}$ drops dramatically because the outlet is sediment starved (Figure 13). The drop in $\frac{Q_s}{Q_t}$ causes $f(Q_s)$ to rise above its new equilibrium value (Figure 14). The rise in $f(Q_s)$ causes incision rates to rise above the new equilibrium value (incision values >1 Figure 15 indicate incision rates that have surpassed the new uplift rate). (Note that incision rates are proportional to $f(Q_s)$, and the trends in Figures 14 and 15 are

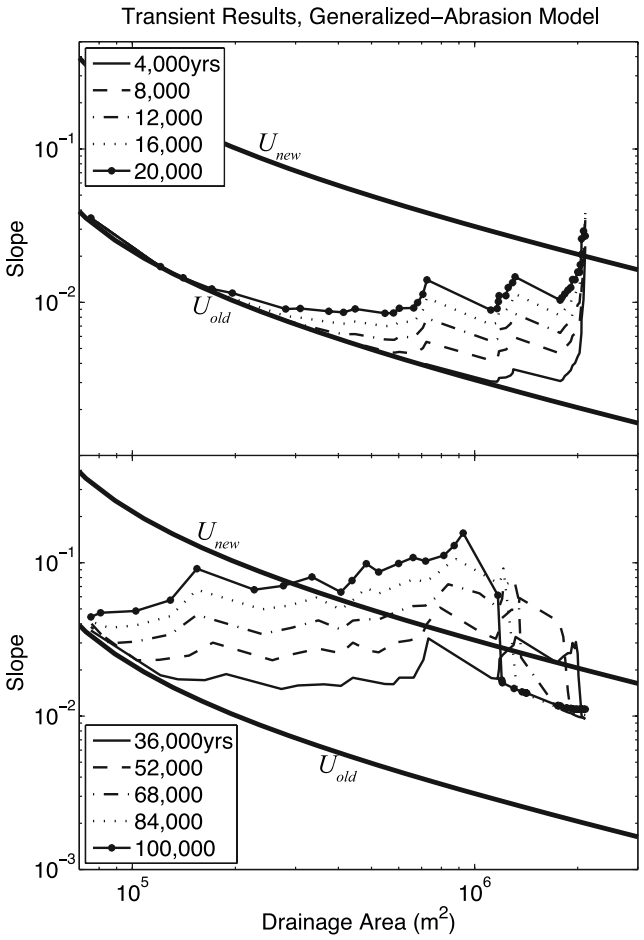

Figure 10. Changes in main channel slope in response to a tenfold increase in uplift rate using the generalized abrasion model. (Parameter values here and in Figures 11–15 are $m = 0.0$, $n = 0.0$, $K_{GA} = 5 \times 10^{-3}$ m^{-1}, $m_t = 1.5$, $n_t = 1$, $K_t = 4 \times 10^{-5}$ yr^{-1}, $k_d = 1$ m^2/yr, $U_{old} = 1 \times 10^{-4}$ m/yr, and $U_{new} = 10 \times 10^{-4}$ m/yr.) As a reference the predicted steady state slope-area relationships with the old and new uplift rates are shown, labeled U_{old} and U_{new}, respectively. Step changes in slope occur where large tributaries join the main channel.

identical.) The large incision rates result in declining channel slopes (Figure 10, bottom) and elevations (Figure 11, bottom).

[60] When the upstream parts of the network begin to respond to the change in uplift rate, the sediment flux downstream begins to rise. The rise in sediment flux causes $\frac{Q_s}{Q_t}$ to rise (Figure 13, bottom) and $f(Q_s)$ and incision rates begin to decrease (Figures 14, bottom, and 15, bottom, respectively). The temporary oversteepening of slopes moves upstream in a wave following the same general pattern as it did near the outlet.

[61] This rise and fall in slopes is similar to the whiplash behavior described by *Gasparini et al.* [2006]. Although we are using a different model in this study, the cause of the whiplash is the same. Initially slopes oversteepen when they are sediment starved in order to keep pace with higher uplift rates. Eventually, as the sediment flux begins to increase and aids in incision, the slopes are able to decrease.

[62] Larger perturbations in uplift rate will cause the slopes to oversteepen at larger drainage areas (equation (36)). We performed a number of experiments on larger networks to test equation (36). We found that in larger networks, even when there is a predicted oversteepening at the outlet, the oversteepening does not always occur. The only way that slopes can oversteepen is for uplift to outpace incision for an extended period of time. If the oversteepening requires a large increase in slope, it also requires a long period of time to oversteepen. During this time, the upper parts of the network begin to respond, nullifying the assumptions used in the derivation of equation (36). However, in many of these cases, even though slopes near the outlet do not oversteepen, the slopes in the upper parts of the network may oversteepen, because they require much less of an uplift increase for oversteepening (equation (36)).

4. Discussion

[63] The saltation-abrasion and generalized abrasion models exhibit a number of unique attributes in both steady state and transient landscapes. Unlike transport-limited or detachment-limited stream power models, the steady state solutions for both the saltation-abrasion and generalized

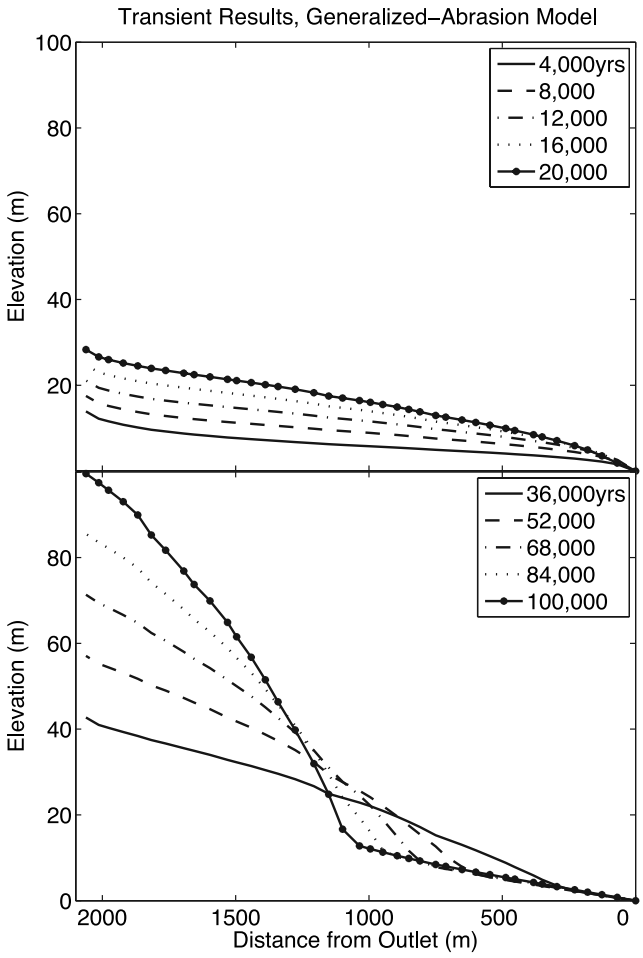

Figure 11. Changes in main channel elevation in response to a tenfold increase in uplift rate using the generalized abrasion model. Corresponding channel slopes are shown in Figure 10. Channel elevations are relative to the point which the network drains to that has a fixed elevation of zero.

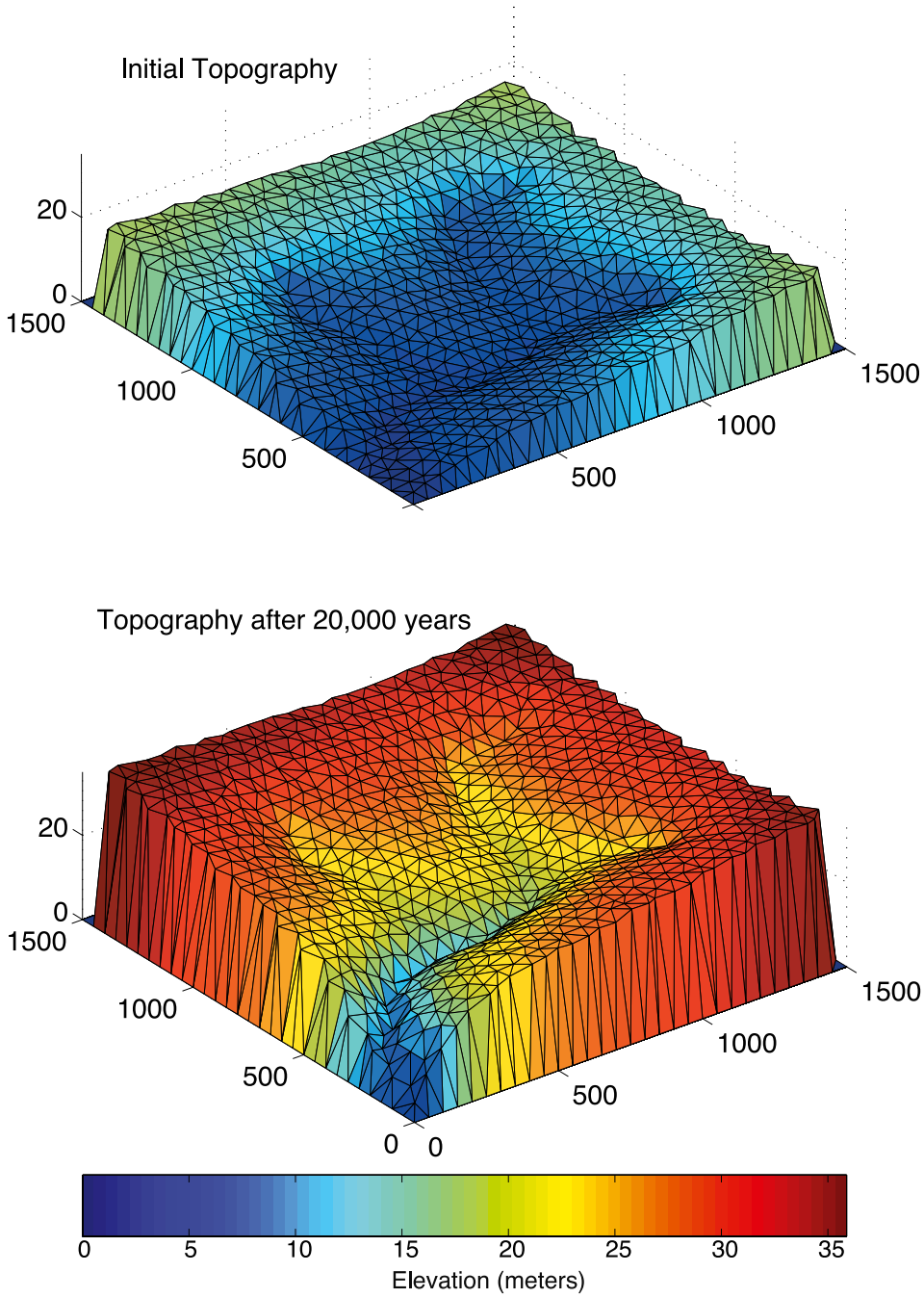

Figure 12. Initial topography and 20,000 years after tenfold increase in uplift rate using the generalized abrasion model. Units on landscape axes are in meters. Landscapes are shaded by elevation, and scale bar on bottom applies to both landscapes. The slope and profile of the main channels are illustrated in Figures 10 and 11. Initial topography, shaded by slope, is illustrated in Figure 4.

abrasion models predict that below a critical drainage area the sediment supply will be too small to produce a fluvial incision rate that keeps pace with the uplift rate. Below this critical drainage area, other processes must dominate erosion. In our numerical experiments we model these processes as diffusive, although this region could be dominated by other processes, such as debris flows [*Stock and Dietrich*, 2003; *Stock et al.*, 2005].

[64] The presence of a threshold area for fluvial processes may be a limitation of the models that we present. Neither the saltation-abrasion nor the generalized abrasion model include processes that do not require sediment for erosion, such as cavitation, weathering, or plucking. Similarly, neither account for suspended load abrasion and processes that focus abrasion in complex bed topography, such as potholing. If these processes were included in the model,

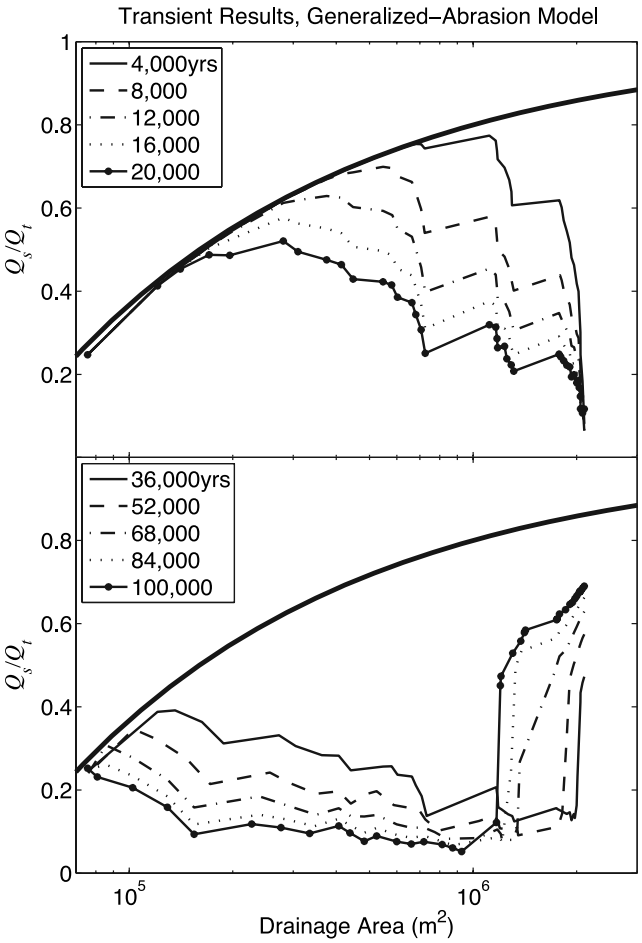

Figure 13. Changes in the ratio of sediment flux to sediment carrying capacity in response to a tenfold increase in uplift rate using the generalized abrasion model. Step changes occur where large tributaries join the main channel. The steady state value does not change with uplift rate and is illustrated by the thick line. Figure 14 illustrates the corresponding changes in $f(Q_s)$ values.

some of the more extreme behavior in drainages with smaller areas might be at least tempered.

[65] However, if the prediction of a critical drainage area is accurate, it has important implications for the sensitivity of drainage density or, similarly, hillslope length. The generalized abrasion model predicts that the critical drainage area is sensitive only to the strength of the bedrock (K_{GA}), while the saltation-abrasion model predicts that the critical drainage area is sensitive to the strength of the bedrock, the climatic conditions and the uplift rate. These are, in principle, testable model predictions for steady state landscapes.

[66] The change in drainage density with uplift rate predicted by the saltation-abrasion model greatly affects the transient landscape response. The conversion of upper reaches from rivers to hillslopes slows down the response in the upper reaches of the network. For example, in the saltation-abrasion simulation, incision rates near the outlet are within 80% of the new steady state rate after 48,000 years (Figure 9). However, even after 200,000 years, incision rates in the uppermost reaches are still slowly increasing and remain below 80% of the new steady state rate. The transient results using the saltation-abrasion model predict that incision rates measured over discrete periods, for example by dating strath terraces [e.g., *Wegmann and Pazzaglia*, 2002], would be much more temporally uniform in the lower reaches than in the upper reaches of the network.

[67] It is possible that during transient conditions other processes that are not modeled here, such as mass wasting, would take over and speed up the transformation of regions that were once fluvial but become hillslopes after an increase in uplift rate. Even if this is the case, the sediment flux models presented here essentially shutdown in the smaller drainages until the hillslopes start to deliver more sediment downstream, or in theory, another process such as mass wasting, starts to occur. Regardless of the process dominating the hillslopes, the upper fluvial reaches are predicted to respond more slowly than the lower reaches of the network because the uplift signal attenuates as it moves upstream. In contrast, the detachment-limited stream

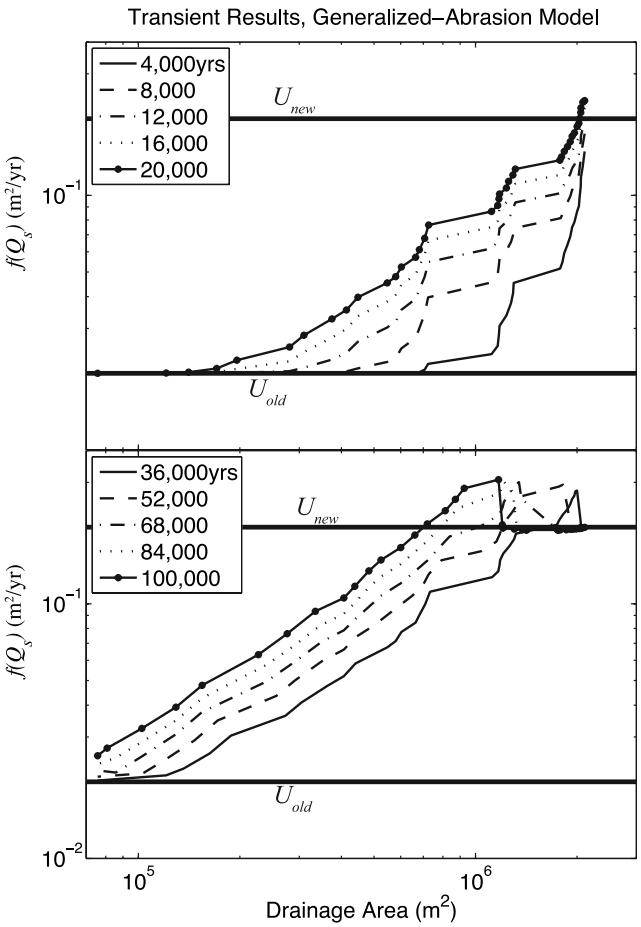

Figure 14. Changes in the sediment flux erodibility in response to a tenfold increase in uplift rate using the generalized abrasion model. Step changes occur where large tributaries join the main channel. As a reference the predicted steady state $f(Q_s)$-area relationships with the old and new uplift rates are shown, labeled U_{old} and U_{new}, respectively. Figure 13 illustrates the corresponding changes in Q_s/Q_t values.

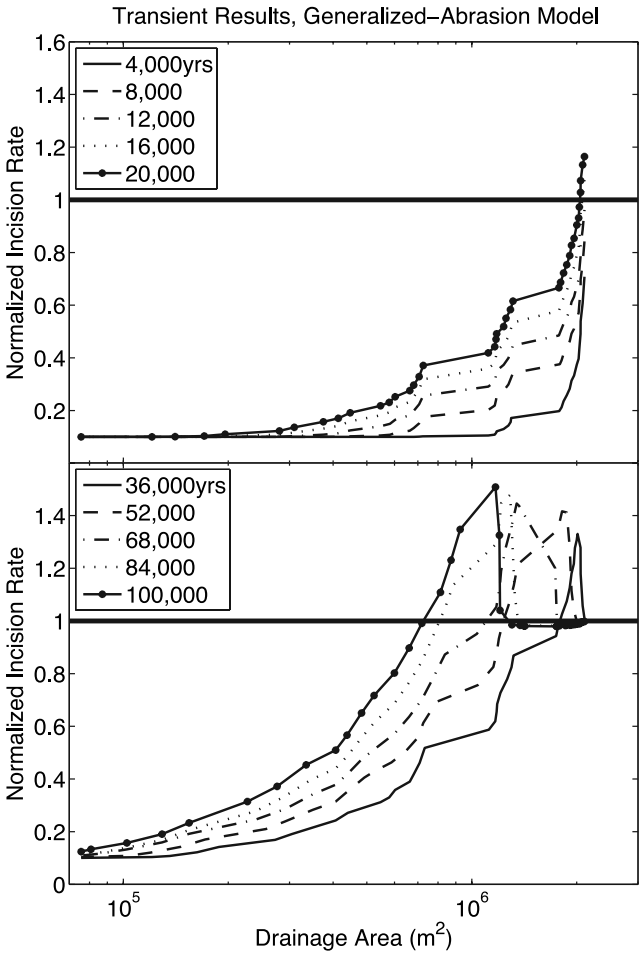

Figure 15. Changes in the incision rate normalized by the new uplift rate using the generalized abrasion model. Values greater than 1 (above the horizontal line) imply that the incision rate has surpassed the uplift rate. The incision rate is averaged over a few thousand years and is not the instantaneous incision rate corresponding to the slope and $f(Q_s)$ values in Figures 10 and 14.

power model never predicts a "shutdown" in fluvial processes during transient conditions and the channel response throughout the network is similar [*Whipple and Tucker*, 2002].

[68] With both models presented here, and the models used by *Gasparini et al.* [2006], the fluvial incision rate at any point in the channel is a function of both the downstream and upstream erosion rates. The response time is a combination of the time that it takes the change in uplift signal to reach the uppermost parts of the fluvial network, the time that it takes for erosion rates to increase on the hillslopes, and the time that it takes the channels to respond to the increase in sediment flux from the both the hillslopes and the upstream channels. In both examples illustrated here, the slope in the downstream part of the network continues to evolve even after the incision rate is very close to the new steady state value. This is a result of the integrated network response, which is not captured using a detachment-limited model [*Whipple and Tucker*, 2002].

[69] The saltation-abrasion model predicts a change in bed cover (as measured by $\frac{Q_s}{Q_t}$) with uplift rate. At steady state, a larger uplift/erosion rate results in less bed cover for a given drainage area (Figure 7). During transients, in general, one would expect that tributaries closer to the mouth of the network, that have had more time to respond to the perturbation in uplift rate, should have less bed cover than tributaries with a similar drainage area that drain into the main channel farther from the outlet, where the uplift perturbation is felt later. These are potentially field testable predictions.

[70] The saltation-abrasion model predicts that during transient conditions $\frac{Q_s}{Q_t}$ initially decreases below its new steady state value, and therefore $\frac{Q_s}{Q_t}$ must increase again at later time (Figure 7). In contrast, the value of $f(Q_s)$ increases throughout the transition because $f(Q_s)$ is not linearly related to $\frac{Q_s}{Q_t}$ (equation (4)). In the downstream reaches, $f(Q_s)$ increases rapidly after the initial perturbation in uplift rate, whereas, at later times the value of $f(Q_s)$ increases more slowly (Figure 8). Field measurements of both $\frac{Q_s}{Q_t}$ and $f(Q_s)$ throughout a channel, which would require measurements of channel width, sediment grain size, channel slope, and other parameters relevant to transport capacity, could be compared with model predictions to provide information on both the bedrock incision model and landscape dynamics.

[71] In all cases that we tested using the saltation-abrasion model, the transient response is similar to the example that we present in this paper. However, the transient response using the generalized abrasion model varies depending on the magnitude of the uplift perturbation. In the example that we illustrate here, there is an oversteepening at the outlet above the new steady state slope, leading to a whiplash effect as channel elevations rise and fall. The area at which oversteepening occurs is predicted by equation (36) and is a function of the variation in uplift rate and the value of K_{GA}.

[72] We performed a number of numerical experiments using the generalized abrasion model in which $A_{GA_{os}}$ was very small (not illustrated here). In these cases, channel slopes change gradually throughout most of the main channel, and the response is similar to the saltation-abrasion response and the transport-limited response, as illustrated by *Whipple and Tucker* [2002]. The main difference between the saltation-abrasion response and generalized abrasion response in these cases is that the generalized abrasion model does not predict changes in drainage density with uplift rate. Therefore, in cases in which the generalized abrasion model predicts a similar response to the saltation-abrasion model, the best location in which to discern between the two models is in the upper reaches of the network. Although the generalized abrasion model predicts that fluvial erosion will be severely limited in the upper reaches as the hillslopes adjust and deliver more sediment to the channels, this model does not predict that channelized regions at low drainage areas will be transformed into hillslopes.

[73] The channel whiplash behavior illustrated by the generalized abrasion model is similar to the behavior predicted by *Gasparini et al.* [2006] using the almost-parabolic model, which is based on the same physical processes described by both *Sklar and Dietrich* [2004] and *Parker* [2004]. The almost-parabolic model differs from the models presented in this paper in that it predicts incision

rates will increase with increasing bed shear stress for a fixed value of $f(Q_s)$, and it does not have a critical drainage area.

[74] The oversteepening of channel slopes predicted by the generalized abrasion model is driven by similar dynamics as those described by *Gasparini et al.* [2006]. Initially, slopes oversteepen near the outlet (Figure 10) so that the incision rate can keep pace with the increase in uplift rate (Figure 15). This oversteepening occurs while much of the upper reaches have not yet had time to respond. Strictly speaking, because the outlet does not respond instantaneously, some adjustment has already taken place in the upper parts of the network by the time the outlet point oversteepens. The exact location of oversteepening is usually at a drainage area smaller than that predicted by equation (36) because adjustments are not instantaneous. As the sediment flux begins to respond, the value of $f(Q_s)$ increases (Figure 14) and the incision rate increases (Figure 15). Once the incision rate surpasses the uplift rate, channel slopes decrease. The mutual adjustment between channel slope and sediment flux leads to a much more dynamic response than would be predicted by a model like the detachment-limited stream power model, which does not depend on the sediment flux, and therefore does not depend on upstream changes in the drainage network.

[75] The saltation-abrasion model never predicts whiplash behavior because of the very narrow range of parameter space that allows reasonable drainage densities at steady state. Any perturbation large enough to drive the saltation-abrasion model away from a transport-limited-like response at large drainage areas would convert the entire landscape into hillslopes because of the relationship between the critical drainage area and uplift rate (equation (26)) (see *Crosby et al.* [2007] for more discussion).

[76] Even though the generalized abrasion model predicts cases in which the channel slope increases and decreases through time, the sediment load at the outlet continually increases throughout the landscape response. Declining channel slopes are normally associated with a decline in transport capacity and therefore a decline in sediment load. However, the integrated network response leads to a steady increase in sediment load at the outlet, even though the local incision rate may decline for a period at some locations in the network. Integrated measurements of network erosion, such as those measured with cosmogenic nuclides [e.g., *Granger et al.*, 1996], would still indicate an overall increase in incision rate in the network, even though incision rates may be declining locally.

[77] Throughout the text we have highlighted a number of observations that we suggest to be field testable in order to gain insight into the dominant fluvial process. The required observations, such as downstream changes in sediment cover, could potentially be masked by other processes and/or more complex transient signals from climate or land use change. We recognize the complications related to making such measurements in natural landscapes, but we also believe that valuable knowledge of the dominant fluvial process can be gleamed from such data, if available.

5. Conclusions

[78] This study discusses the steady and nonsteady state morphologies predicted by two different bedrock incision models based on the work by *Sklar and Dietrich* [2004] and *Parker* [2004] that include the effects of wear by saltating bed load. We find that there are a number of differences between these models and the commonly used detachment-limited stream power model [e.g., *Whipple and Tucker*, 1999]. Many of the model predictions are potentially field testable and can be used to discern between models and also to infer information on the magnitude and type of perturbation experienced in a nonsteady state landscape.

[79] 1. At steady state, both abrasion models predict that there is a critical drainage area below which the steady state sediment load is too small to produce an incision rate that keeps pace with the uplift rate. Below this critical drainage area, other processes must dominate erosion. In the saltation-abrasion model the critical drainage area is a function of uplift rate, climate, and bedrock strength; in the generalized abrasion model the critical drainage area is solely a function of the bedrock strength.

[80] 2. At steady state, both abrasion models converge to a transport-limited solution at large drainage areas. The steady state slope in these models is only discernible from the transport-limited slope at smaller drainage areas, which have steeper slopes and a larger concavity than predicted by the transport-limited solution.

[81] 3. Both abrasion models predict a longer transient response in comparison with the detachment-limited stream power model. The fluvial response in both abrasion models is dependent on the delivery of sediment from upstream, including sediment delivery from the hillslopes.

[82] 4. The saltation-abrasion model (in all cases) and the generalized abrasion model (in some cases) both predict that the transient response in much of the trunk channel will be similar to a transport-limited response [*Whipple and Tucker*, 2002]. This result implies that the absence of knickpoints alone may not necessarily indicate that a network has reached steady state.

[83] 5. Both models predict that bed cover varies during a transition from low to high uplift rate. Measurements of bed cover in different regions of the network can be indicative of the bedrock incision model, and of the state of evolution of the landscape.

[84] 6. Both models are most sensitive to sediment delivery from the hillslopes in the headwaters of the network. These reaches may be the best locations to determine to what extent the fluvial incision rate is controlled by the sediment flux.

[85] 7. The generalized abrasion model predicts a very dynamic response in the main channel to large increases in uplift rate. The model predicts that channel slopes may rise and fall in response to a single increase in uplift rate, similar to the results presented by *Gasparini et al.* [2006]. This implies that declining slopes are not necessarily indicative of declining incision rates.

Notation

A	drainage area [L^2].
$\mathbf{A_{GA_c}}$	steady state critical drainage area, generalized abrasion model [L^2].
$A_{GA_{os}}$	area at which slopes oversteepen, generalized abrasion model [L^2].

$A_{GA_{trans}}$ transient critical drainage area, generalized abrasion model [L^2].
$\mathbf{A_{SA_c}}$ steady state critical drainage area, saltation-abrasion model [L^2].
$A_{SA_{trans}}$ transient critical drainage area, saltation-abrasion model [L^2].
b area exponent in width equation (dimensionless).
β fraction of incoming sediment load transported as bed load (dimensionless).
c area exponent in fluvial discharge equation (dimensionless).
D diameter of sediment [L].
ε_v rock resistance to abrasion [$M\,L^{-1}T^{-2}$].
f roughness parameter from Darcy-Weisbach equation (dimensionless).
$f(Q_s)$ sediment flux erodibility [L^2T^{-1}]
g acceleration of gravity [LT^2].
H hillslope erosion rate [LT^{-1}].
H_s saltation height [L].
I bedrock incision rate [LT^{-1}].
$\mathbf{I}$ steady state bedrock incision rate [LT^{-1}].
I_{GA} bedrock incision rate calculated using generalized abrasion model [LT^{-1}].
$\mathbf{I_{GA}}$ steady state bedrock incision rate predicted by generalized abrasion model [LT^{-1}].
I_{SA} bedrock incision rate calculated using saltation-abrasion model [LT^{-1}].
$\mathbf{I_{SA}}$ steady state bedrock incision rate predicted by saltation-abrasion model [LT^{-1}].
k_d hillslope diffusivity coefficient [L^2T^{-1}].
k_q fluvial discharge coefficient [$L^{3-2c}T^{-1}$].
k_τ basal shear stress coefficient [$ML^{-5/3}T^{-2}$].
k_w width coefficient [$L^{3b-1}T^{-b}$].
K bedrock incision coefficient, incision equation [$L^{-(2m+1)}$].
K_t bed load transport capacity coefficient [$L^{3-2m_t}\,T^{-1}$].
K_{GA} bedrock incision coefficient, generalized abrasion model [L^{-1}].
K_{SA} bedrock incision coefficient, saltation-abrasion model [$L^{-0.5}$].
L_s saltation hop length [L].
λ ratio of new rock uplift rate to old rock uplift rate (dimensionless).
m area exponent, incision equation (dimensionless).
m_t area exponent, sediment transport capacity equation (dimensionless).
n slope exponent, incision equation (dimensionless).
n_t slope exponent, sediment transport capacity equation (dimensionless).
w_{si} vertical component of particle velocity at the bed, [LT^{-1}].
Q fluvial discharge [L^3T^{-1}].
Q_s incoming sediment flux [L^3T^{-1}].
$\mathbf{Q_s}$ steady state incoming sediment flux [L^3T^{-1}].
Q_t sediment transport capacity [L^3T^{-1}].
ρ water density [ML^{-3}].
r fraction of the particle volume detached from bed per particle collision (dimensionless).
R_b submerged specific gravity (dimensionless).
S channel slope (dimensionless).
$\mathbf{S_{new}}$ steady state slope after an increase in uplift (dimensionless).
$\mathbf{S_{GA}}$ steady state slope, generalized abrasion model (dimensionless).
$S_{GA_{trans}}$ transient slope, generalized abrasion model (dimensionless).
$\mathbf{S_{SA}}$ steady state slope, saltation-abrasion model (dimensionless).
$\mathbf{S_{TL}}$ steady state slope, transport-limited model (dimensionless).
t time [T].
τ basal shear stress [$M\,L^{-1}T^{-2}$].
τ^* Shield's stress (dimensionless)
τ_c critical shear stress for sediment entrainment [$M\,L^{-1}T^{-2}$].
τ_c^* critical Shield's stress (dimensionless)
u_s average horizontal component of particle velocity [LT^{-1}].
U rock uplift rate [LT^{-1}].
U_{new} rock uplift rate after increase in uplift rate [LT^{-1}].
U_{old} rock uplift rate before increase in uplift rate [LT^{-1}].
W channel width [L].
z channel elevation [L].

[86] **Acknowledgments.** This work was funded by the NASA Earth System Science Fellowship and the Yale University Bateman Postdoctoral Fellowship. Discussions with Mark Brandon, Ben Crosby, and Greg Tucker were helpful in formulating this work. We thank Bob Anderson, Alan Howard, and an anonymous reviewer for their thoughtful comments.

References

Beaumont, C., P. Fullsack, and J. Hamilton (1992), Erosional control of active compressional orogens, in *Thrust Tectonics*, edited by K. R. McClay, pp. 1–18, CRC Press, Boca Raton, Fla.

Brandon, M. T., and N. M. Gasparini (2005), A power-law approximation for fluvial incision by tools and bed coverage processes, *Eos Trans. AGU*, *86*(52), Fall Meet. Suppl., Abstract H53D-0515.

Crosby, B. T., K. X. Whipple, N. M. Gasparini, and C. W. Wobus (2007), Formation of fluvial hanging valleys: Theory and simulation, *J. Geophys. Res.*, doi:10.1029/2006jf000566, in press.

Fernandez Luque, R., and R. van Beek (1976), Erosion and transport of bedload sediment, *J. Hydraul. Res.*, *14*(2), 127–144.

Finnegan, N. J., G. Roe, D. R. Montgomery, and B. Hallet (2005), Controls on the channel width of rivers: Implications for modeling fluvial incision of bedrock, *Geology*, *33*(3), 229–232.

Gasparini, N. M., G. E. Tucker, and R. L. Bras (2004), Network-scale dynamics of grain-size sorting: Implications for downstream fining, stream-profile concavity and drainage basin morphology, *Earth Surf. Processes Landforms*, *29*, 401–421.

Gasparini, N. M., R. L. Bras, and K. X. Whipple (2006), Numerical modeling of non-steady-state river profile evolution using a sediment-flux-dependent inicision model, in *Tectonics, Climate and Landscape Evolution*, edited by S. D. Willett et al., *Spec. Pap. Geol. Soc. Am.*, *398*, 127–141.

Gilbert, G. K. (1877), Report of the geology of the Henry Mountains, technical report, 160 pp., U.S. Geol. Surv., Reston, Va.

Granger, D. E., J. W. Kirchner, and R. C. Finkel (1996), Spatially averaged long-term erosion rates measured from in-situ produced cosmogenic nuclides in alluvial sediment, *J. Geol.*, *104*, 249–257.

Hancock, G. S., and R. S. Anderson (2002), Numerical modeling of fluvial strath-terrace formation in response to oscillating climate, *Geol. Soc. Am. Bull.*, *114*, 1131–1142.

Hancock, G. S., R. S. Anderson, and K. X. Whipple (1998), Beyond power: Bedrock river incision process and form, in *Rivers Over Rock: Fluvial Processes in Bedrock Channels*, *Geophys. Monogr. Ser.*, vol. 107, edited by K. J. Tinkler and E. E. Wohl, pp. 35–60, AGU, Washington, D. C.

Hartshorn, K., N. Hovius, W. B. Dade, and R. L. Slingerland (2002), Climate-driven bedrock incision in an active mountain belt, *Science*, *297*, 2036–2038.

Hilley, G. E., M. R. Strecker, and V. A. Ramos (2004), Growth and erosion of fold-and-thrust belts with an application to the Aconcagua fold-and-thrust belt, Argentina, *J. Geophys. Res.*, *109*, B01410, doi:10.1029/2002JB002282.

Howard, A. D. (1980), Thresholds in river regimes, in *Thresholds in Geomorphology*, edited by D. R. Coates and J. D. Vitek, pp. 227–258, Allen and Unwin, St. Leonards, N. S. W., Australia.

Howard, A. D. (1994), A detachment-limited model of drainage basin evolution, *Water Resour. Res.*, *30*, 2261–2285.

Howard, A. D., and G. Kerby (1983), Channel changes in badlands, *Geol. Soc. Am. Bull.*, *94*, 739–752.

Howard, A. D., M. A. Seidl, and W. E. Dietrich (1994), Modelling fluvial erosion on regional to continental scales, *J. Geophys. Res.*, *99*, 13,971–13,986.

Kirkby, M. J. (1986), A two-dimensional simulation model for slope and stream evolution, in *Hillslope Processes*, edited by A. D. Abrahams, pp. 203–222, Allen and Unwin, St. Leonards, N. S. W., Australia.

Komar, P. D., and Z. Li (1986), Pivoting analyses of the selective entrainment of sediments by shape and size with application to gravel threshold, *Sedimentology*, *33*, 425–436.

Kooi, H., and C. Beaumont (1994), Escarpment evolution on high-elevation rifted margins: Insights derived from a surface processes model that combines diffusion, advection, and reaction, *J. Geophys. Res.*, *99*, 12,191–12,209.

Leopold, L. B., and T. Maddock (1953), The hydraulic geometry of stream channels and some physiographic implications, *U.S. Geol. Surv. Prof. Pap.*, *252*, 1–57.

Meyer-Peter, R., and R. Müller (1948), Formulas for bedload transport, in *Proceedings of 2nd Meeting International Association of Hydraulic Research*, pp. 39–64, Int. Assoc. of Hydraul. Eng. and Res., Madrid.

Molnar, P. (2001), Climate change, flooding in arid environments, and erosion rates, *Geology*, *29*, 1071–1074.

Montgomery, D. R., and K. B. Gran (2001), Downstream variations in the width of bedrock channels, *Water Resour. Res.*, *37*, 1841–1846.

Morris, P. H., and D. J. Williams (1997), Exponential longitudinal profiles of streams, *Earth Surf. Processes Landforms*, *22*, 143–163.

O'Connor, J., and J. E. Costa (2004), Spatial distribution of the largest rainfall-runoff floods from basins between 2.6 and 26,000 km^2 in the United States and Puerto Rico, *Water Resour. Res.*, *40*, W01107, doi:10.1029/2003WR002247.

Parker, G. (1991), Selective sorting and abrasion of river gravel. I: Theory, *J. Hydraul. Eng.*, *117*(2), 131–149.

Parker, G. (2004), Somewhat less random notes on bedrock incision, *Internal Memo. 118*, St. Anthony Falls Lab., Univ. of Minn.–Twin Cities, Minneapolis. (Available at http://cee.uiuc.edu/people/parkerg/reports.htm)

Roe, G. H., D. B. Stolar, and S. D. Willett (2006), Response of a steady-state critical wedge orogen to changes in climate and tectonic forcing, in *Tectonics, Climate and Landscape Evolution*, edited by S. D. Willett et al., *Spec. Pap. Geol. Soc. Am.*, *398*, 227–239.

Roering, J. J., J. W. Kirchner, and W. E. Dietrich (2001), Hillslope evolution by nonlinear, slope-dependent transport: Steady state morphology and equilibrium adjustment timescales, *J. Geophys. Res.*, *106*, 16,499–16,513.

Rosenbloom, N. A., and R. S. Anderson (1994), Hillslope and channel evolution in a marine terraced landscape, Santa Cruz, California, *J. Geophys. Res.*, *99*, 14,013–14,029.

Shields, A. (1936), Application of similarity principles and turbulence research to bedload movement, translated from German by W. P. Caott and J. C. Uchelen, *Rep. 167*, 43 pp., W. M. Keck, Lab. of Hydraul. and Water Resour., Calif. Inst. of Technol., Pasadena.

Sinha, S. K., and G. Parker (1996), Causes of concavity in longitudinal profiles of rivers, *Water Resour. Res.*, *32*, 1417–1428.

Sklar, L. (2003), The influence of grain size, sediment supply, and rock strength on rates of river incision into bedrock, Ph.D. thesis, 343 pp., Univ. of Calif., Berkeley.

Sklar, L., and W. E. Dietrich (1998), River longitudinal profiles and bedrock incision models: Stream power and the influence of sediment supply, in *Rivers Over Rock: Fluvial Processes in Bedrock Channels*, *Geophys. Monogr. Ser.*, vol. 107, edited by K. J. Tinkler and E. E. Wohl, pp. 237–260, AGU, Washington, D. C.

Sklar, L., and W. E. Dietrich (2001), Sediment and rock strength controls on river incision into bedrock, *Geology*, *29*, 1087–1090.

Sklar, L., and W. E. Dietrich (2004), A mechanistic model for river incision into bedrock by saltating bed load, *Water Resour. Res.*, *40*, W06301, doi:10.1029/2003WR002496.

Slingerland, R., K. Furlong, and J. W. Harbaugh (1994), *Simulating Clastic Sedimentary Basins*, 220 pp., Prentice-Hall, Upper Saddle River, N. J.

Snow, R. S., and R. L. Slingerland (1987), Mathematical modeling of graded river profiles, *J. Geol.*, *95*, 15–33.

Snyder, N. P., K. X. Whipple, G. E. Tucker, and D. J. Merritts (2000), Landscape response to tectonic forcing: Digital elevation model analysis of stream profiles in the Mendocino triple junction region, northern California, *Geol. Soc. Am. Bull.*, *112*(8), 1250–1263.

Snyder, N. P., K. X. Whipple, G. E. Tucker, and D. J. Merritts (2003a), Importance of a stochastic distribution of floods and erosion thresholds in the bedrock river incision problem, *J. Geophys. Res.*, *108*(B2), 2117, doi:10.1029/2001JB001655.

Snyder, N. P., K. X. Whipple, G. E. Tucker, and D. M. Merritts (2003b), Channel response to tectonic forcing: Analysis of stream morphology and hydrology in the Mendocino triple junction region, norther California, *Geomorphology*, *53*, 97–127.

Solyom, P. B., and G. E. Tucker (2004), Effect of limited storm duration on landscape evolution, drainage basin geometry, and hydrograph shapes, *J. Geophys. Res.*, *109*, F03012, doi:10.1029/2003JF000032.

Stock, J., and W. E. Dietrich (2003), Valley incision by debris flows: Evidence of a topographic signature, *Water Resour. Res.*, *39*(4), 1089, doi:10.1029/2001WR001057.

Stock, J. D., D. R. Montgomery, B. D. Collins, W. E. Dietrich, and L. S. Sklar (2005), Field measurements of incision rates following bedrock exposure: Impliciations for process controls on the long profiles of valleys but by rivers and debris flows, *Geol. Soc. Am. Bull.*, *117*(1/2), 174–194.

Tomkin, J. H., M. T. Brandon, F. J. Pazzaglia, J. R. Barbour, and S. D. Willett (2003), Quantitative testing of bedrock incision models for the Clearwater River, NW Washington state, *J. Geophys. Res.*, *108*(B6), 2308, doi:10.1029/2001JB000862.

Tucker, G. E. (2004), Drainage basin sensitivity to tectonic and climatic forcing: Implications of a stochastic model for the role of entrainment and erosion thresholds, *Earth Surf. Processes Landforms*, *29*, 185–205.

Tucker, G. E., and R. L. Bras (1998), Hillslope processes, drainage density, and landscape morphology, *Water Resour. Res.*, *34*, 2751–2764.

Tucker, G. E., and R. L. Slingerland (1996), Predicting sediment flux from fold and thrust belts, *Basin Res.*, *8*, 329–349.

Tucker, G. E., and R. L. Slingerland (1997), Drainage basin responses to climate change, *Water Resour. Res.*, *33*, 2031–2047.

Tucker, G. E., and K. X. Whipple (2002), Topographic outcomes predicted by stream erosion models: Sensitivity analysis and intermodel comparison, *J. Geophys. Res.*, *107*(B9), 2179, doi:10.1029/2001JB000162.

Tucker, G. E., S. T. Lancaster, N. M. Gasparini, and R. L. Bras (2001a), The channel-hillslope integrated landscape development model (CHILD), in *Landscape Erosion and Evolution Modeling*, edited by R. S. Harmon and W. W. Doe, pp. 349–388, Springer, New York.

Tucker, G. E., S. T. Lancaster, N. M. Gasparini, R. L. Bras, and S. M. Rybarczyk (2001b), An object-oriented framework for distributed hydrologic and geomorphic modeling using triangulated irregular networks, *Comput. Geosci.*, *27*, 959–973.

van der Beek, P., and P. Bishop (2003), Cenozoic river profile development in the upper Lachlan catchment (SE Australia) as a test of quantitative fluvial incision models, *J. Geophys. Res.*, *108*(B6), 2309, doi:10.1029/2002JB002125.

Wegmann, K. W., and F. J. Pazzaglia (2002), Holocene strath terraces, climate change, and active tectonics: The Clearwater River basin, Olympic Peninsula, Washington State, *Geol. Soc. Am. Bull.*, *114*(6), 731–744.

Whipple, K. X. (2004), Bedrock rivers and the geomorphology of active orogens, *Annu. Rev. Earth Planet. Sci.*, *32*, 151–185.

Whipple, K. X., and B. J. Meade (2004), Controls on the strength of coupling among climate, erosion, and deformation in two-sided, frictional orogenic wedges at steady state, *J. Geophys. Res.*, *109*, F01011, doi:10.1029/2003JF000019.

Whipple, K. X., and G. E. Tucker (1999), Dynamics of the stream-power river incision model: Implications for height limits of mountain ranges, landscape response timescales, and research needs, *J. Geophys Res.*, *104*, 17,661–17,674.

Whipple, K. X., and G. E. Tucker (2002), Implications of sediment-flux-dependent river incision models for landscape evolution, *J. Geophys. Res.*, *107*(B2), 2039, doi:10.1029/2000JB000044.

Whipple, K. X., G. S. Hancock, and R. S. Anderson (2000a), River incision into bedrock: Mechanics and relative efficacy of plucking, abrasion, and cavitation, *Geol. Soc. Am. Bull.*, *112*, 490–503.

Whipple, K. X., N. P. Snyder, and K. Dollenmayer (2000b), Rates and processes of bedrock incision by the Upper Ukak River since the 1912 Novarupta ash flow in the Valley of Ten Thousand Smokes, Alaska, *Geology*, *28*, 835–838.

Wilcock, P. R. (1998), Two-fraction model of initial sediment motion in gravel-bed rivers, *Science*, *280*, 410–412.

Willgoose, G., R. L. Bras, and I. Rodriquez-Iturbe (1991), Results from a new model of river basin evolution, *Earth Surf. Processes Landforms*, *16*, 237–254.

Wilson, K. C. (1966), Bedload transport at high shear stresses, *J. Hydraul. Eng.*, *92*(6), 49–59.

Wohl, E. E. (1993), Bedrock channel incision along Piccanniny Creek, Australia, *J. Geol.*, *101*, 749–761.

Wohl, E. E. (1998), Bedrock channel morphology in relation to erosional processes, in *Rivers Over Rock: Fluvial Processes in Bedrock Channels*, *Geophys. Monogr. Ser.*, vol. 107, edited by K. J. Tinkler and E. E. Wohl, pp. 133–151, AGU, Washington, D. C.

Wohl, E. (2004), Limits of downstream hydraulic geometry, *Geology*, *32*(10), 897–900.

R. L. Bras, Department of Civil and Environmental Engineering, Massachusetts Institute of Technology, Cambridge, MA 02139, USA.

N. M. Gasparini and K. X. Whipple, School of Earth and Space Exploration, Arizona State University, Tempe, AZ 85287, USA. (nicoleg@alum.mit.edu)